NRIM SR-94-01

Environmentally Assisted Cracking of Structural Materials for Light Water Reactors

by

Norio NAGATA

NRIM Special Report
(Research Report)
No. 94–01

1994

National Research Institute for Metals
2–3–12, Nakameguro, Meguro-ku, Tokyo, Japan

NRIM SR-94-01

Environmentally Assisted Cracking of Structural Materials for Light Water Reactors

by

Norio NAGATA

NRIM Special Report
(Research Report)
No. 94–01

1994

National Research Institute for Metals
2–3–12, Nakameguro, Meguro-ku, Tokyo, Japan

Environmentally Assisted Cracking of Structural Materials for Light Water Reactors

by
Norio NAGATA

NRIM Special Report
(Research Report)
No. 94–01

Contents

Abstract 1
1. Introduction 2
2. Environmental Degradation of LWR Components 2
  2.1 SCC of Austenitic Stainless Steel Piping 2
  2.2 SCC and CF of SG Tubing 3
  2.3 Fatigue Failure in Carbon Steel Piping 3
  2.4 CF of Low Alloy Steel for RPV 3
3. Framework of EAC Research by NRIM 3
4. Experimental Techniques 3
5. SCC of Structural Materials for LWRs 8
  5.1 SCC of Austenitic Stainless Steels 9
    5.1.1 Temperature dependence 9
    5.1.2 Effect of heating and cooling rates 10
    5.1.3 Effect of environmental and loading transients 10
    5.1.4 Role of oxide film on SCC 11
  5.2 SCC of High Nickel Alloys 12
  5.3 SCC of Carbon Steels 13
6. CF of Low Alloy Steels 16
  6.1 Low Cycle Fatigue 16
    6.1.1 Effect of high temperature water environment on S-N curves 17
    6.1.2 Comparison with ASME Code, Sec. III 18
    6.1.3 Origin of fatigue cracking in high temperature water 18
  6.2 Fatigue Crack Growth 19
    6.2.1 Direct observation of cracking in high temperature water 19
    6.2.2 Effects of variables on fatigue crack growth rates 20
  6.3 Interaction of CF and SCC in Low Alloy Steel 27
7. Mechanism of EAC in LWR Coolant Environments 28
8. Application of EAC Data 28
9. Concluding Remarks 29
Acknowledgements 30
References 30

Environmentally Assisted Cracking of Structural Materials for Light Water Reactors

by

Norio NAGATA*

Abstract

Materials used in nuclear power plants respond to the surrounding coolant environment, frequently resulting in serious damage to the integrity of reactor components. Some of this damage is cracking of reactor pressure vessels, piping and steam generator tubes due to corrosion fatigue and stress corrosion cracking. This paper presents an overview of research on environmentally assisted cracking of structural materials for light water reactors based on work conducted by NRIM for more than a decade. NRIM has made a major effort to define the influential factors, especially environmental, for the degradation of materials under high temperature water environments that simulate LWR coolants. Carbon steels, low alloy steels, austenitic stainless steels and nickel base alloys were examined. Corrosion fatigue behavior of the low alloy steels was analyzed with the ASME Boiler and Pressure Vessel Code, Section III design fatigue curves and with the reference curves in ASME Code, Section XI, Appendix A to evaluate the margin of material strength in high temperature water environments. The stress corrosion cracking behavior of the materials tested was analyzed in terms of environmental factors such as dissolved oxygen concentration, strain rate, and temperature. The results are available for the revision of codes and plant operation procedures to keep nuclear power plants safe.

Keywords: *corrosion fatigue, stress corrosion cracking, carbon steels, low alloy steels, austenitic stainless steels, nickel base alloys, high temperature water environment, light water reactor*

* Supervising Researcher of 5th Research Group. From April 1st, 1994 associated with Nuclear Safety Technology Center (NUSTEC).

1. Introduction

The capacity of nuclear power plants in Japan now exceeds a quarter of the total electrical power generation, and plant operation is so stable that it is applauded worldwide. Nuclear energy is expected as a reliable and stable energy resource in Japan, which has inherently poor domestic resources for energy. Unfortunately, however, severe accidents have been experienced by plants at Three Mile Island and Chernobyl. Since no commercial nuclear power plant has yet ended its plant life, the safety of nuclear power plants throughout their life should be of worldwide concern.

The materials for structural components in nuclear power plants require the highest soundness and reliability, being one of the fundamental elements of the system. Light water reactors (LWR), which comprise the majority of commercial nuclear power plants, have experienced damage due to stress corrosion cracking (SCC) of primary recirculation piping and steam generator (SG) tubes[1]. Damage of materials in nuclear power plants reduces the plant reliability and brings enormous economic loss. To raise the safety and reliability of nuclear power plants, the behavior of structural materials in coolant environments, and especially materials for the primary pressure boundary which comprises the confinement of radioactive materials, should be comprehensively understood and reflected in the design and safe operation of the plants. From this viewpoint, NRIM has conducted the national program on safety research for LWRs since 1980 and promoted research on corrosion fatigue (CF) and stress corrosion cracking (SCC) of the materials for reactor pressure vessels (RPV), coolant piping and SG tubes for reactor pressure boundaries of domestic reactors. This paper describes results obtained through work conducted by NRIM for the safety research program of nuclear reactor materials. Research at NRIM has followed four sub-themes: 1) CF of low alloy steels for RPV, 2) SCC of ferritic steels and austenitic stainless steels for the primary pressure boundary, 3) SCC of nickel base alloys for SG tubes and 4) SCC of Zircalloy for fuel cladding. Work has aimed at quantitatively defining influential factors, such as mechanical, environmental and metallurgical, on the initiation and growth of cracks in simulated reactor environments, analyzing the damage mechanisms and establishing information for the evaluation and prediction of cracking of materials in coolant environments. However, a description of the SCC of Zircalloy was omitted from the discussion of environmentally assisted cracking (EAC) behavior under coolant environments.

2. Environmental Degradation of LWR Components

LWRs have so far experienced various kinds of accidents and originating from material degradation under service conditions. A few examples of plant accidents that have triggered research on EAC problems are introduced below.

Causes of materials failures occurring in nuclear power plants are:

1) SCC in stainless steel piping of boiling water reactor (BWR),
2) SCC in stainless steels weldments,
3) Irradiation assisted SCC (IASCC),
4) Corrosion damage of steam generator tubing of pressurized water reactor (PWR),
5) CF and thermal fatigue of carbon steels,
6) Erosion/corrosion and
7) Fretting fatigue of PWR SG tubing.

Typical examples of cracking failures due to fatigue and SCC are as follows:

2.1 SCC of Austenitic Stainless Steel Piping

In the middle to the end of the 1970s, many BWR plants, not only in the United States but also in Japan, were shut down due to intergranular SCC (IGSCC) of Types 304 and 316 austenitic stainless steel piping. Worldwide cooperative research brought about the successful remedy for IGSCC of stainless steels, based on knowledge of the SCC mechanism. This mechanism requires the combination of a sensitized austenitic structure, tensile stress and high dissolved oxygen content in the coolant environment. Remedies such as reduction of the carbon content of alloys, reduction of the residual stress from welding, suppression of sensitization, and reduction of the dissolved oxygen (DO) concentration recovered the integrity of the plant components. However, SCC damage still occurs in austenitic stainless steel components, probably because of the interaction of high residual stress and the existence of crevice.

2.2 SCC and CF of SG Tubing

Nickel base Alloy 600 is widely used for SG tubes of PWR in Japan and the USA. Since 1977, some of SG components have suffered from corrosion damage called intergranular attack (IGA) from secondary coolants. IGA is considered to be the result of intergranular corrosion and SCC due to alkaline densification at tube/plate gaps. Remedies such as the substitution of volatile alkaline for solid alkalines, the use of optimum heat treatments for the tubing, and the use of Alloy 690 nickel base alloy for new tube materials have reduced the problems.

2.3 Fatigue Failure in Carbon Steel Piping

Through-wall cracks in secondary feed water nozzles of PWR steam generators in the USA in early 1980s were suspected to be due to high cycle fatigue in a corrosive environment[2]. Thermal striping also caused thermal fatigue failure of horizontal piping. The latter is considered to be due to thermal fluctuations caused by the cyclic replacement of cold water by leakage through shutdown valves.

2.4 CF of Low Alloy Steel for RPV

The RPV is the most important component of a nuclear power plant and must have superior integrity throughout the plant life. One of most probable causes of RPV damage is fatigue. The first case of cracking occurring in an operating RPV was at the JPDR of the Japan Atomic Energy Research Institute (JAERI), where fine cracks were discovered on the inner wall by inspection.

JAERI started a study of cracking in pure water at high temperature and pressure and found an acceleration of crack growth due to the environment[3, 4]. The JAERI study was historic because it triggered not only domestic research, but also a worldwide cooperative research effort on corrosion fatigue, called the International Cooperative group on Cyclic Crack Growth Rate (ICCGR)[5].

3. Framework of EAC Research by NRIM

Corrosion of metals and alloys is one of the major research subjects that NRIM has struggled with since its establishment in 1956. Materials and environments are important factors for the study of corrosion, and corrosion problems in nuclear reactor materials were selected for research since the beginning of NRIM. Since then, NRIM has engaged in studying corrosion problems such as the general corrosion of aluminum alloys, stainless steels, and zirconium alloys in high temperature water environments. Study of SCC of austenitic stainless steels in high temperature water started in 1962, initially using static autoclave systems, then recirculating autoclave systems and slow extension testers. In the middle of the 1970's, malfunctions of BWR plants by failure of primary recirculation piping due to SCC, as mentioned above, was common in the world and triggered the enthusiastic study of SCC at NRIM. SCC problems of zirconium alloys for fuel cladding by fission products such as iodine were also studied. In the early 1980's, the Nuclear Safety Commission of Japan established and promoted a nation-wide research program for nuclear safety, in which NRIM was the major institute for materials research. In this program, NRIM built a framework for the study of environmentally assisted cracking, such as CF and the SCC of structural materials for primary pressure boundary components of LWRs, that has continued for over a decade. As is well known, EAC is governed by three major factors: materials, mechanics and environment. NRIM mainly stressed the effect of corrosive environments on cracking failure because the trend of EAC research seemed to lean more to mechanical factors, such as the effect of stress ratio on fatigue crack propagation or strain rate on fatigue life, in the high temperature water environment. The present overview describes the results obtained from the nuclear safety research program for LWR materials conducted by NRIM during the recent decade, including related results from previous works.

4. Experimental Techniques

LWRs use plain light water for the neutron moderator and coolant. Since water is used under high pressure and temperature conditions (e.g., 7.3 MPa at 561 K for BWR or 16.0 MPa at 595 K for PWR), a high temperature, pressurized water autoclave is necessary for simulation of coolant environments at all flow rates. In addition, the water recirculation system must feed the test environment with the specified water chemistry. NRIM has installed many test apparatuses for conducting CF and SCC tests in high temperature water. Figs. 1 and 2 are schematic

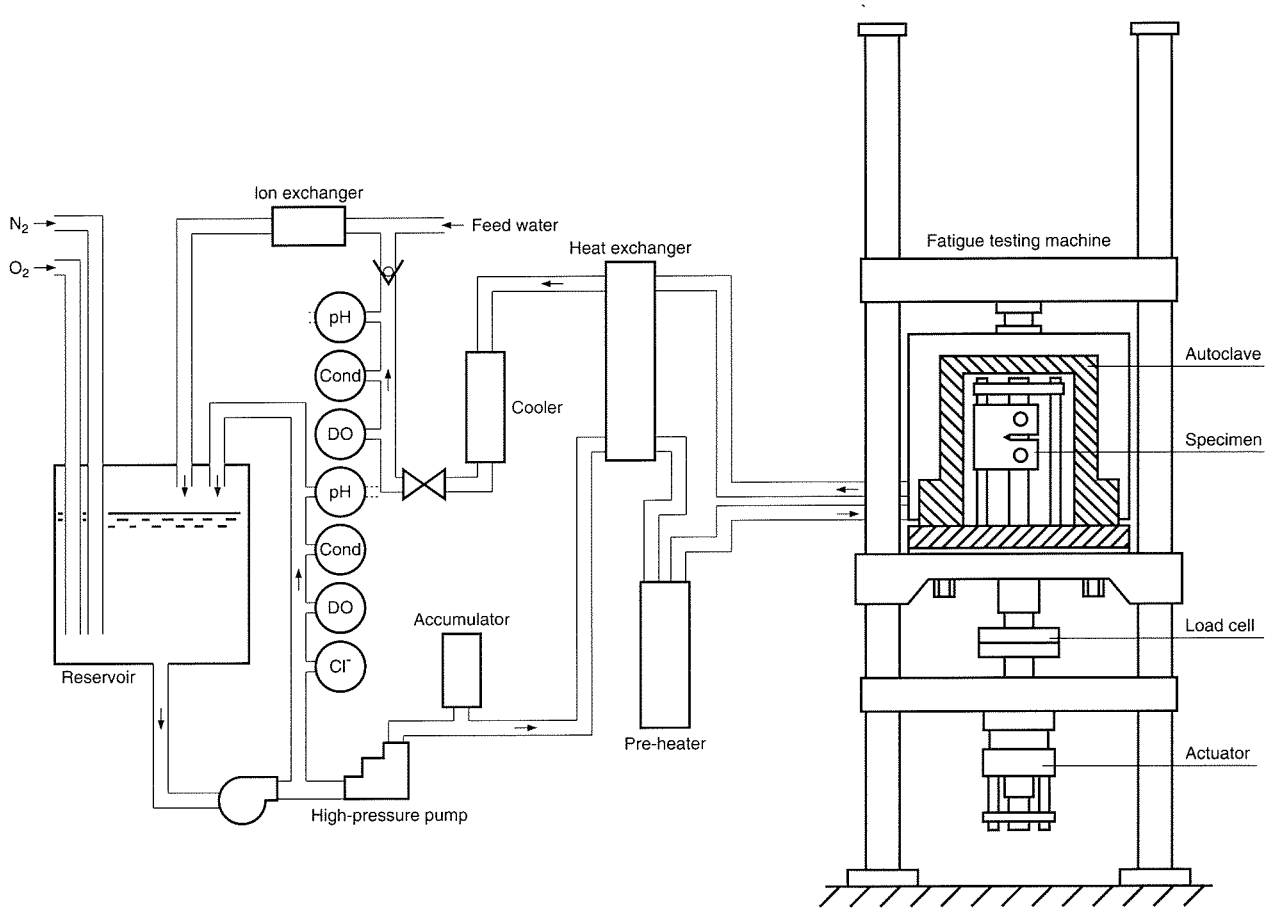

Fig. 1 Schematic diagram of corrosion fatigue testing machine

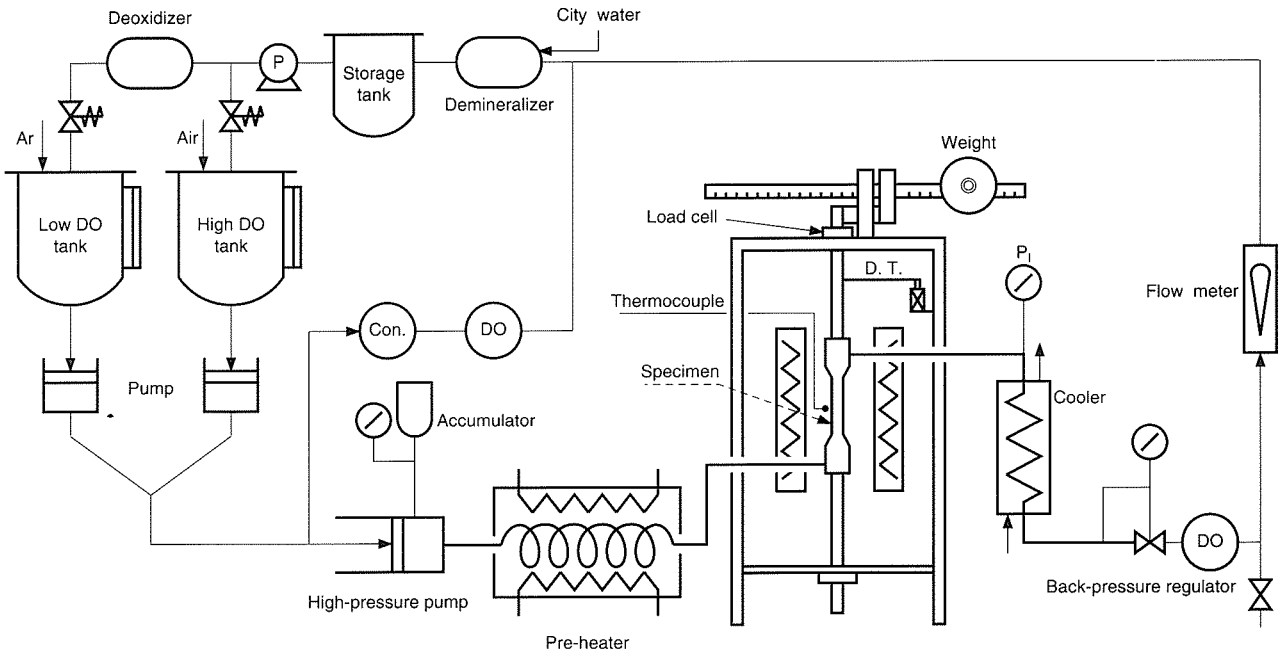

Fig. 2 Schematic diagram of SCC testing machine

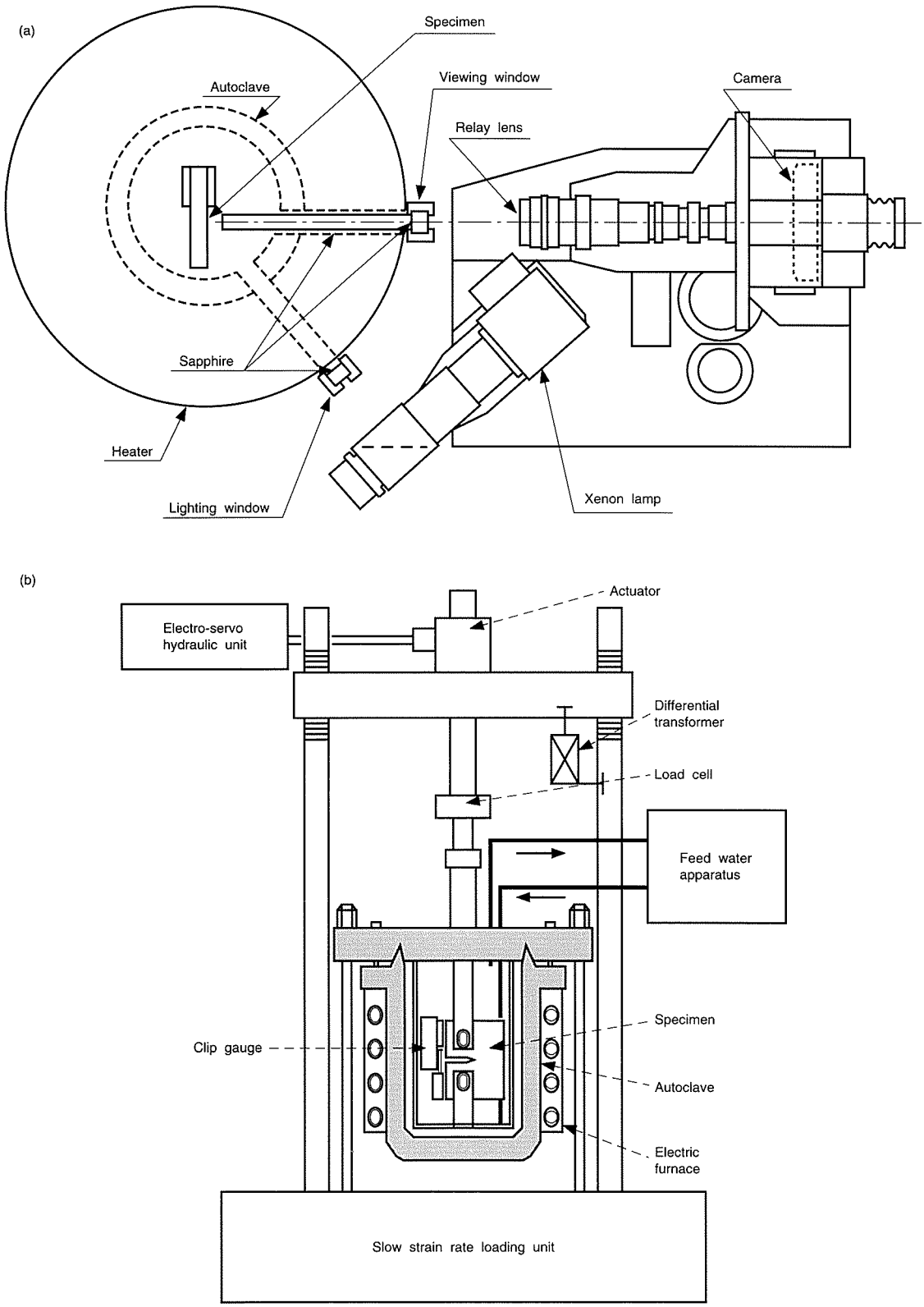

Fig. 3 Modification of EAC testing machines. (a) Schematic top view of the optical observation system and (b) Testing machine for CF-SCC interaction

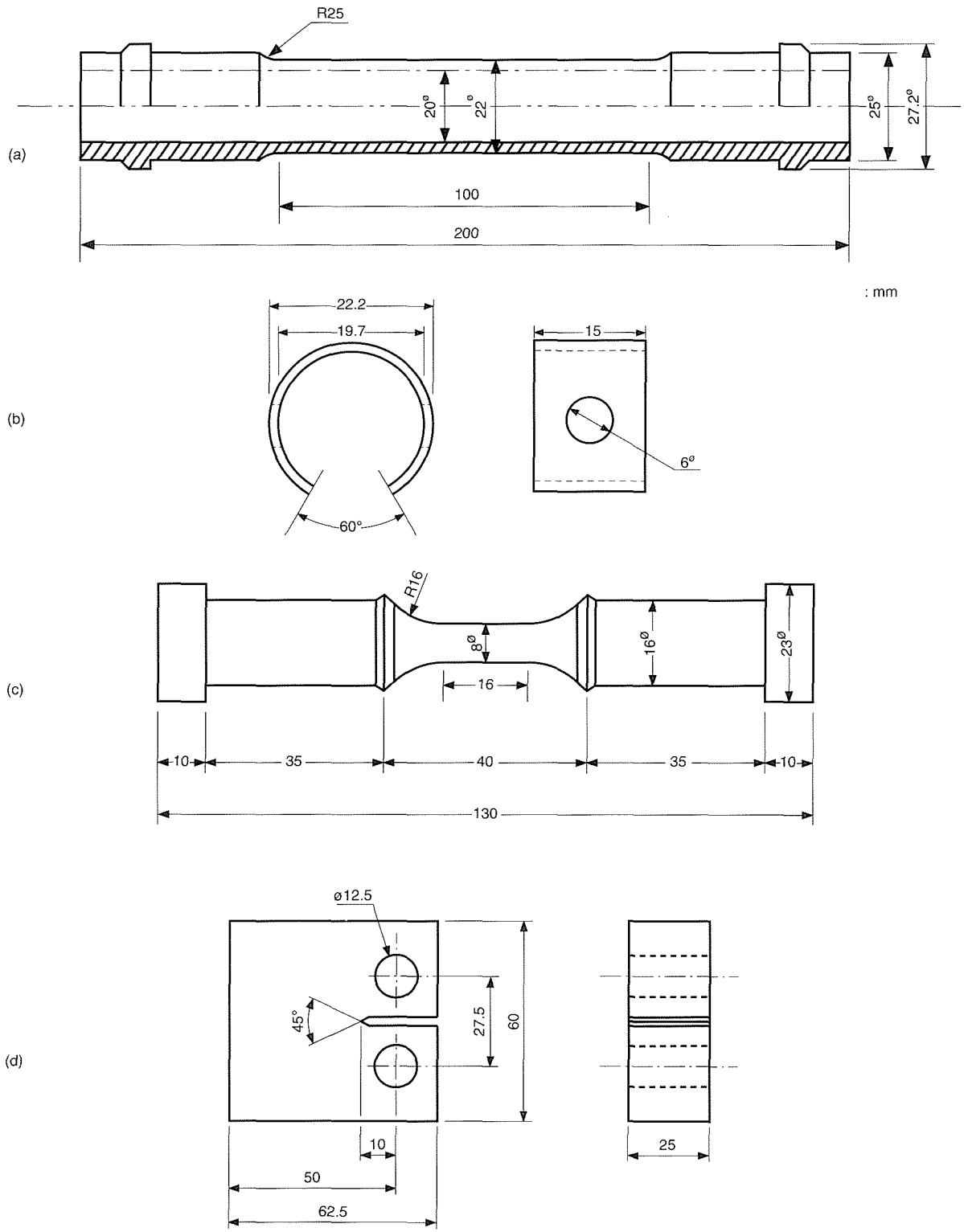

Fig. 4 Specimen dimensions (mm). (a) Tubular specimen for SCC test, (b) C-ring specimen for SCC test, (c) Round bar specimen for low cycle fatigue test and (d) CT specimen for crack growth test

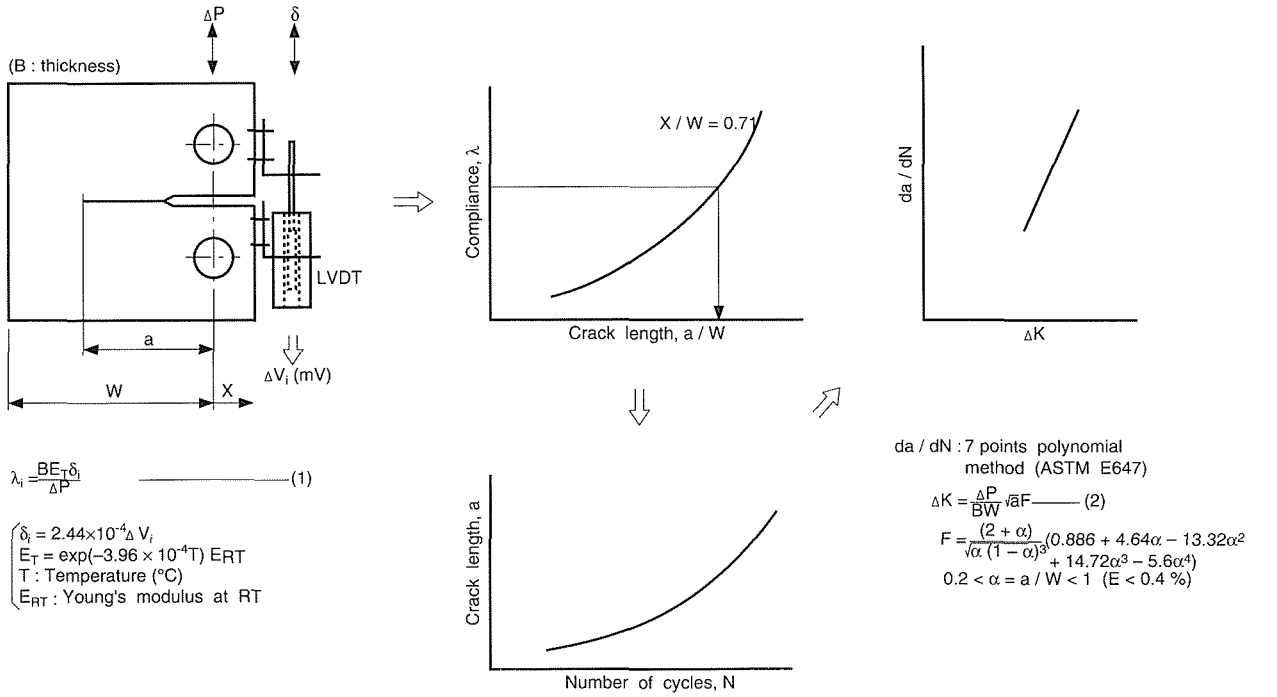

Fig. 5 Schematic reduction of crack growth data by compliance method

representations of a typical CF tester and SCC tester, respectively, that include an autoclave and water recirculation system. Although these have been used mainly for ordinary material characterization tests, such as fatigue life, fatigue crack growth rate, SCC susceptibility, and corrosion, the equipment was also modified to provide additional information, such as the direct observation of cracking of specimens in an autoclave and tests with the superposition of cyclic and slow extension loads. The latter was designed to study CF-SCC interactions. The system for the direct observation of cracking is illustrated in Fig. 3(a), while the loading device for superposition of cyclic and slow extension loads is shown in Fig. 3(b).

Dimensions of specimens employed for slow strain rate tests (SSRT) and C-ring tests for SCC, low cycle fatigue tests and fatigue crack growth tests are given in Fig. 4. The tubular specimen shown in Fig. 4(a) was employed for SCC tests under bi-axial loading to simulate small schedule piping in power plants. This experimental procedure presents a capability of SCC test without using autoclave for the case of, for instance, the direct contact of wave guide bars to the specimen.

Standard compact tension (1TCT) specimens following ASTM E399[6] were used for crack growth tests, while large scale CT specimens were used for optical observation of cracking in high temperature water. The large CT specimens were cut from thick, reactor pressure vessel plates following ASTM E647[7] and had a thickness of 25 mm and width of 120 mm. A compliance method, which used a linear variable differential transformer (LVDT) produced in the USA by Schaevitz Co. was employed for crack length measurements of specimens in the autoclave. Fig. 5 shows a schematic illustration of the compliance method and the data reduction procedure. Care was taken to ensure reliability of the reduced crack length for use in linear fracture mechanics[8]. For this purpose, the specimen crack length in an autoclave was measured directly and compared to estimates using the compliance method. Details of this method are described in 6.2.1.

The total strain imposed on the specimen during low cycle fatigue tests was measured and controlled using a pair of differential transformers. The magnetic cores were put in sheaths in the pressure boundary and connected through extension rods to circumferential projections on the roots of the specimen, as shown in Fig. 4(c). The total strain of the test section was calibrated using a reference curve that was determined in advance. Measurement and

Table 1 Chemical composition, heat treatment and mechanical property of materials tested

Alloys	Chemical compositions (wt%)											Heat treatment	Mechanical properties (R. T.)			
	C	Si	Mn	P	S	Ni	Cr	Fe	Mo	V	Cu		Y. S. (MPa)	U. T. S. (MPa)	El. (%)	R. A. (%)
Carbon steel (JIS:STPT42)	0.20	0.22	0.51	0.024	0.016			Bal.				As received	280.3	453.7	31.5	
Carbon steel (JIS:STS42)	0.16	0.14	1.20	0.026	0.015			Bal.				1173 K × 10 min A. C.	353	539	36	
A508 C1.3 (JIS:SFVQ1A)	0.17	0.28	1.38	0.003	0.003	0.74	0.15	Bal.	0.48	0.003		1259 – 1295 K × 7 h 15 min W. Q. 940 – 952 K × 7 h 45 min A. C. 883 K × 23 h F. C.	447	598	29.1	73
A508 C1.3												1143 – 1173 K ×7 h 15 min W. Q. 923 – 933 K × 7 h 30 min A. C. After welding 907 K × 26 h 30 min F. C.				
Base metal	0.18	0.20	1.40	0.003	0.003	0.74	0.17	Bal.	0.47	0.003			442	589	25	71
Weld metal	0.07	0.30	1.13	0.008	0.005	0.84	0.07	Bal.	0.46	0.001	0.03		502	585	29	
Welding bar	0.09	0.19	1.64	0.006	0.005	0.90	0.07	Bal.	0.45	<0.001	0.02					
A533B C1.1 (JIS:SQV2A) Low Sulfer	0.19	0.24	1.28	0.008	0.007	0.64	0.19	Bal.	0.45	tr.	0.04	1273 K W. Q. 955 K × 5 h F. C. 897 K × 45 h F. C.	454	601	29.0	68
A533B C1.1 (JIS:SQV2A) Medium Sulfer	0.21	0.29	1.45	0.007	0.014	0.65	0.03	Bal.	0.51		0.03	1173 K × 7 h W. Q. 933 K × 5 h A. C. 873 K × 25 h F. C.	475	629	22	61
Type 304 Plate	0.07	0.55	1.01	0.013	0.018	8.68	18.03	Bal.	0.20		0.06	1323 K × 0.5 h W. Q. 923 K × 2 h F. C.				
Tube	0.067	0.45	1.82	0.029	0.014	9.52	18.36	Bal.	0.25		0.26	1323 K × 0.5 h W. Q. 923 K × 2 h F. C.	230	692	68	
Type 316	0.07	0.61	1.01	0.024	0.005	12.18	16.75	Bal.	2.30		0.29	923 K × 1 h F. C.				
Alloy 800												As received				
Plate	0.017	0.49	0.82	0.010	0.002	33.95	21.30	Bal.		Ti: 0.48						
Tube	0.019	0.45	0.73	0.006	0.013	33.36	21.85	Bal.		Ti: 0.65						
Alloy 600	0.02	0.13	0.23		0.006	Bal.	16.7	8.49				1423 K × 0.5 h A. C. (923 K × 5 h F. C.)				

control of the strain at the specimen test section was also attempted by using knife-edge rods, but the device was found to be unstable in the autoclave.

Water chemistry is the most influential factor in the environmental degradation of materials. The most serious but controllable chemical is dissolved oxygen (DO). The DO concentrations studied included the range from the saturated concentration to 1 ppb. We made a special effort to control the dissolved oxygen concentration in the test water as strictly as possible by bubbling with nitrogen or argon/oxygen mixed gas into water during the test. Although it took time for the DO concentration to stabilize, transient fluctuations of the DO concentration were less than about 10% to 20% of the set point, even at the lowest concentration of 1 ppb.

The materials tested were those used for the pressure boundary of LWRs, such as low alloy steels for RPV, carbon and austenitic stainless steels for piping, and nickel-base alloys for SG heat exchanger tubes. Details of compositions, heat treatments and strength properties are listed in Table 1.

5. SCC of Structural Materials for LWRs

Stress corrosion cracking (SCC) is one of the significant EAC mechanisms for the failure of LWR components and structures in other fields of engineering technology. Originally, the coolants employed for LWRs, and especially the pure water used for BWRs, were considered to be moderate for the materials used for these components, but a number of SCC failures have been experienced in nuclear power plants. NRIM was interested in SCC phenomena as a damage process of LWR component failure at the early stages of these problems and took up the challenge to study the SCC mechanism. Most SCC failures in LWR components took place in Types 304 and 316 austenitic stainless steels and Alloy 600 nickel base alloys. It is well known that SCC occurs with the combination of three controlling factors, i.e. sensitization of the material, tensile stress and necessary environmental conditions. NRIM concentrated on the effect of environmental factors, such as dissolved oxygen and temperature, in addition to the effects of heat treat-

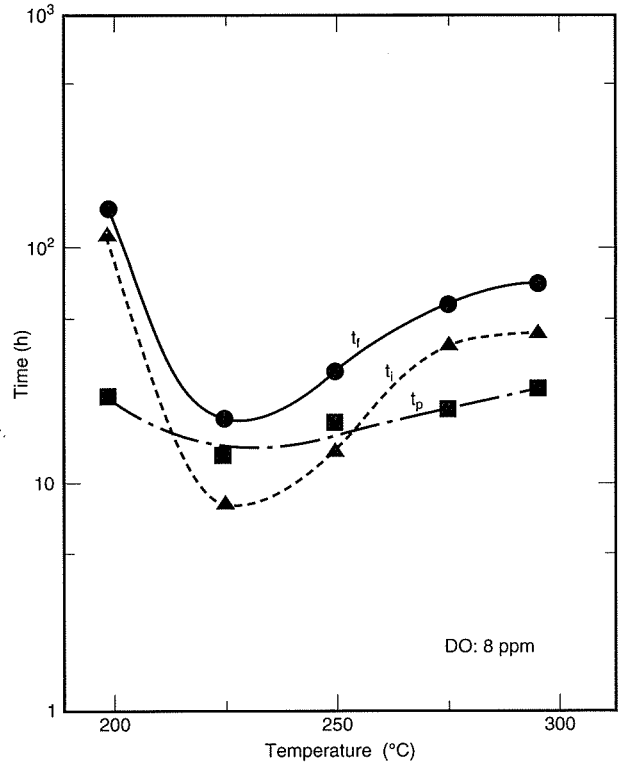

Fig. 6 Effect of temperature on crack initiation time t_i, propagation time t_p and fracture time t_f for Type 304 stainless steel in stagnant water containing 8 ppm DO

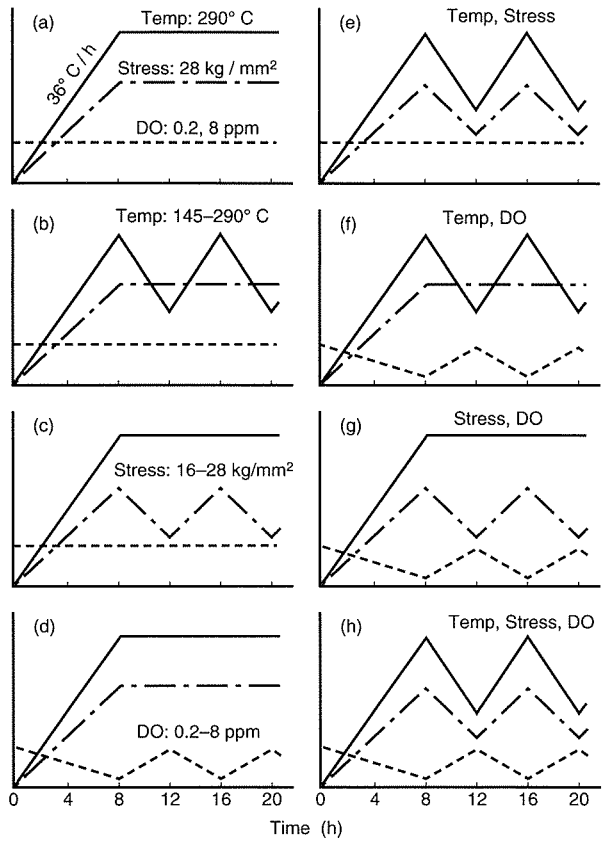

Fig. 7 Combinations of cyclic changes in water temperature, DO concentration and stress for SCC tests

ment and mechanical factors. Our deep understanding of SCC phenomena of structural materials for the pressure boundary components of LWRs are summarized below.

5.1 SCC of Austenitic Stainless Steels

Austenitic stainless steels are commonly used for LWR components such as pressure vessel overlays and piping for recirculation and clean up systems. Of the problems that have so far occurred in nuclear power plants, intergranular SCC in the heat affected zone of BWR primary recirculation system weldments in the mid 1970s was one of the most serious. These SCC problems triggered a world-wide study of SCC of stainless steels in coolant environments. IGSCC of piping was eliminated by modification of the materials, welding procedures and water chemistry. The research on SCC of nuclear materials commenced at NRIM in advance of the SCC problems of BWRs, and some fundamental knowledge of the SCC behavior of stainless steels in high temperature water environments had already been obtained.

5.1.1. Temperature dependence

NRIM tried to clarify the SCC process by analyzing the elongation-time relations of austenitic stainless steels in view of environmental effects such as water temperature, chloride ion concentration and pH. Cracking failure of materials can be divided into two terms, crack initiation and crack propagation. Fig. 6[9] shows the temperature dependence of the time to crack initiation t_i and of crack propagation t_p of 304 stainless steel in stagnant water containing 8 ppm DO. A minimum in the fracture time t_f is apparent around 498 K in accordance with t_i and t_p. This implys that the SCC susceptibility of 304 stainless steel increases during the start up and shut down operation. Similar results were also observed in water with chloride ion addition[10]. It is well known that austenitic stainless steels have a high susceptibility to SCC in neutral water containing chloride ions at high temperatures, and that the cracking is closely associated with pitting formation. The present study also confirmed

evidence that SCC originated from corrosion pits. Since the time for SCC initiation correlates with that for the initiation of pitting, the earliest occurrence of SCC around 473 K should correlate with the early formation of corrosion pits at this temperature. This is because the corrosion pit potential at this temperature is the most cathodic potential that gives rise to pitting. The reason for the reduction of SCC at temperatures above 523 K might be due to the temperature dependence of the pitting corrosion potential in addition to the oxide film protection effect.

5.1.2. Effect of heating and cooling rates

In addition to the above work, we examined the effect of heating and cooling rates on SCC behavior of 304 and 316 austenitic stainless steels by means of U-bend test[11]. It was found by varying the heating rate from 35 K/h to 140 K/h and the chloride ion concentration from 30 ppm to 300 ppm that the probability of SCC occurring increased with decreasing heating rate and with increasing chloride ion concentration. The U-bend specimen cracked during heating when the heating rate was below the critical. Complete SCC occurrence was found for the conditions of 70 K/h at 300 ppm Cl^- and 35 K/h at 100 ppm Cl^- for solution annealed 304 stainless steel, and at any rate above 50 ppm Cl^- for sensitized 304 stainless steel. No SCC was observed for 316 stainless steel under the conditions of a heating rate above 93 K/h at 300 ppm Cl^- or for any rate at 100 ppm Cl^-. On the other hand, cooling rates varying from 30 K/h to 300 K/h had no effect on SCC occurrence for either steel. We concluded from these results that the process temperature of components made of 304 stainless steel should avoid or minimize the time in the temperature range of 473–523 K to the extent possible for start-up or operations with temperature gradients in this range. This is metallurgical evidence of an SCC problem for the present operating management of nuclear power plants.

5.1.3. Effect of environmental and loading transients

Correlation between plant start-up/shut-down operations and the occurrence of SCC was found by an investigation of nuclear plants that had experienced SCC failures[12]. From this background, NRIM examined the effects of transients in environmental factors and loading

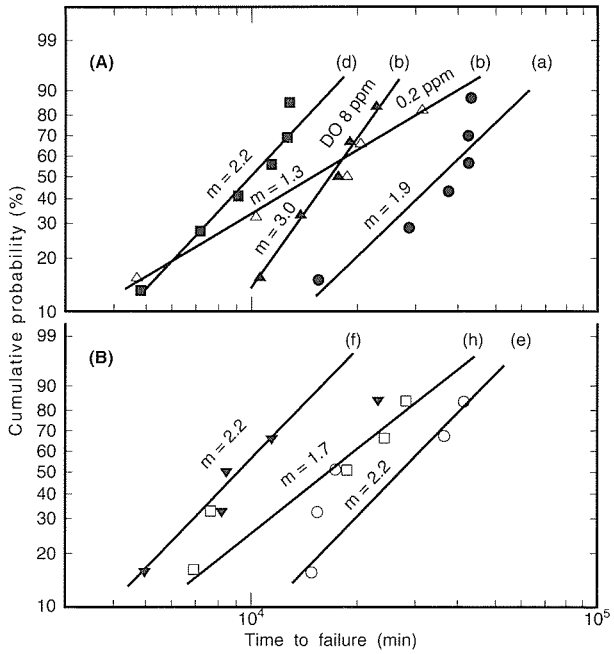

Fig. 8 Weibull distribution of failure time of SCC for Type 304 stainless steel in high temperature water under the conditions of Fig. 7

on the occurrence of SCC in sensitized 304 stainless steel by simulating plant operations. The modes of simulated transients of temperature, DO and stress with time are shown in Fig. 7[13]. In this experiment, tubular test specimens and the test equipment introduced in Figs. 4(a) and 2, were used. Since a previous report indicated that the SCC failures obeyed a Weibull distribution, the cumulative probability of all the test results were analyzed, as shown in Fig. 8[13]. The mean time to failure obtained by the linear relationship in this figure is listed in Table 2. As seen in the figure and the table, the most effective factor was DO concentration. The earliest occurrence of SCC was found under a combination of temperature and DO concentration. SCC did not occur under cyclic stress but did occur under steady state loading. We made additional experiments with lower loading rates and reached the conclusion that the initial loading mode, not the cyclic strain rate, was important. This is in agreement with the literature[14], which maintains the importance of cyclic loading. The SCC behavior under the transient modes studied indicates that control of the temperature and DO concentration of the coolant during start-up operations is important for preventing the occurrence of SCC.

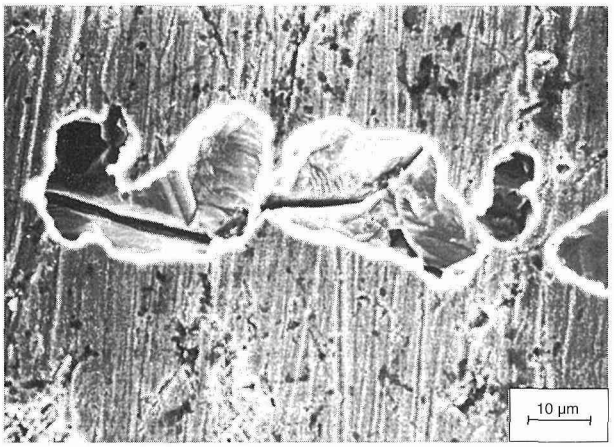

Fig. 9 Specimen surface after anodic dissolution test in 0.5 mol/L H_2SO_4 + 0.05 mol/L KSCN solution using prefilmed specimen exposed to 8 ppm DO water at 523 K

Table 2 Median time to failure of sensitized Type 304 stainless steel tested under the conditions of Fig. 7

Test conditions		MTTF* (min)
(a)	DO 8 ppm	38270
	DO 0.2 ppm	6×10^4 NF**
(b)	DO 8 ppm	16790
	DO 0.2 ppm	18600
(c)	DO 8 ppm	6×10^4 NF
(d)		10180
(e)	DO 8 ppm	28339
(f)		9830
(g)		6×10^4 NF
(h)		18900

* Median time to failure
** No failure

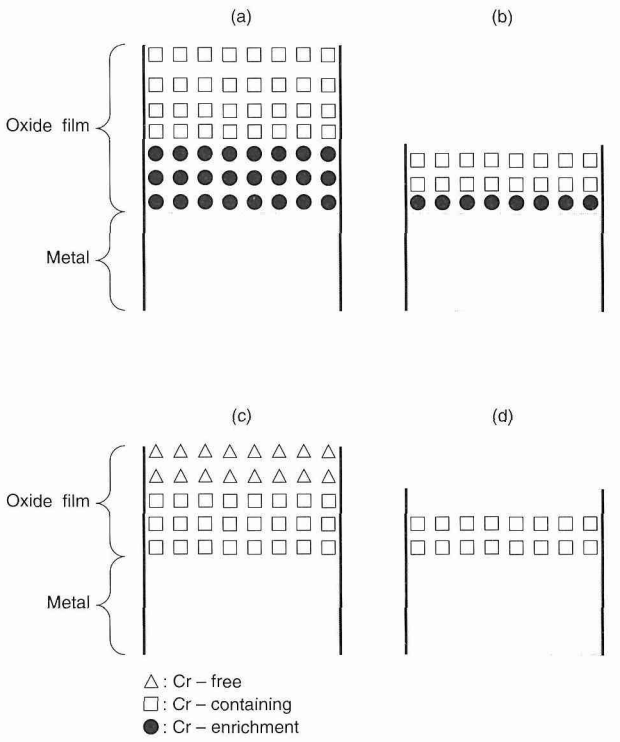

Fig. 10 Schematic illustration of oxide films formed on the grain surface and Cr-depleted regions of Type 304 stainless steel in high temperature water. (a) Oxide film on grain and (b) Cr-depleted region in low DO concentration(~0.2 ppm); (c) Oxide film on grain and (d) Cr-depleted region in high DO concentration (≥ 2 ppm)

5.1.4. Role of oxide film on SCC

The previous section described the influence of the environment and loading on the SCC behavior of sensitized 304 stainless steel, in which the combination of cyclic variations of temperature and DO brought about the earliest SCC failure. Since a thick oxide film forms on the metal surface in high temperature water containing high DO concentrations, the fracture behavior of the oxide film might influence the SCC behavior of stainless steels. Fig. 9[15] shows the surface of a sensitized 304 specimen with an oxide film. The film was formed in high temperature water containing 8 ppm DO followed by an anodic polarization treatment. The picture shows evidence of the localized dissolution of the oxide film beneath which IGSCC takes place. The anodic polarization behavior confirmed that the weakness of the oxide film on the grain boundaries is correlated with the depletion of chromium along the grain boundaries in the matrix by sensitization. The oxide film formed in water with 8 ppm DO had depth profiles that show the depletion of chromium and low porosity, while that formed in water with 0.2 ppm DO showed an enriched chromium content and a high porosity that had seven times the specific surface area determined by the BET isothermal adsorption method than the 8 ppm DO profile. Based on this, we proposed the idea of a duplex structure with an oxide film formed on the surface of the matrix and a chromium-depleted region of sensitized 304 stainless steel, as illustrated schematically in Fig. 10[15]. Fig. 11[15] is a conclusive illustration of the relation between the oxide film behavior and IGSCC susceptibility. The susceptibility can be controlled by the dissolution behavior of the oxide film, i.e., by the peak current density (I_{max}) in the active

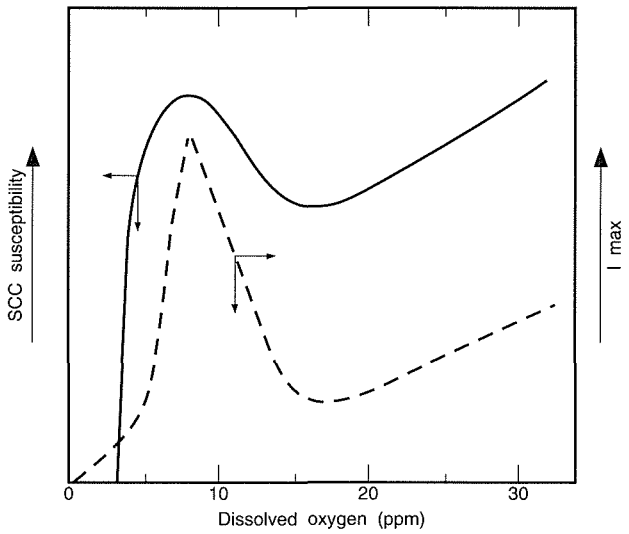

Fig. 11 Schematic illustration of the effect of DO concentration on IGSCC susceptibility and the anodic peak current density for oxide film dissolution

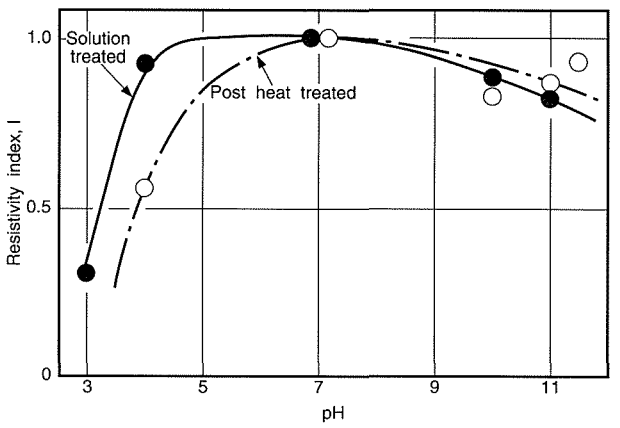

Fig. 12 Effect of pH on resistivity index of Alloy 600 in 8 ppm DO water at 573 K

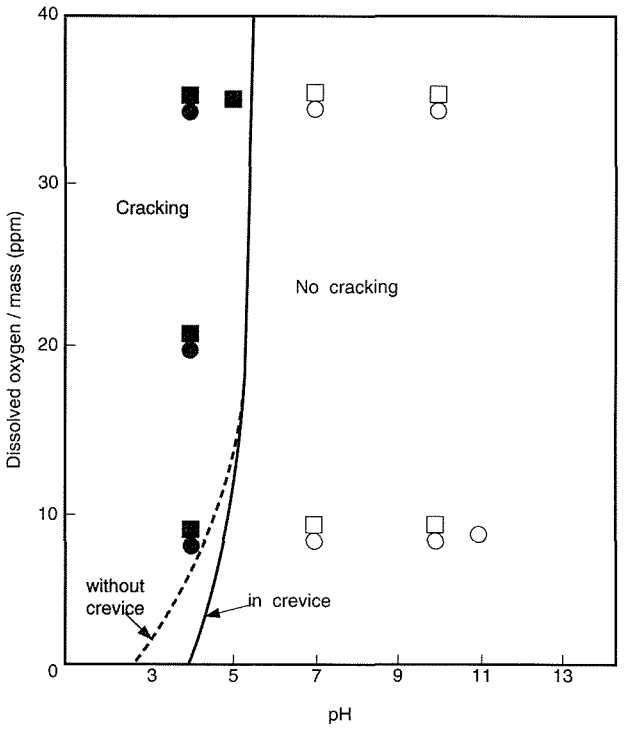

Fig. 13 Effect of DO concentration and pH in high temperature water on SCC susceptibility of Alloy 600. ○●: without crevice, □■: with crevice

state, which is a sum of the dissolution of the oxide film and the dissolution of the metal matrix through thin parts of the oxide film. In other words, IGSCC susceptibility of the sensitized 304 stainless steel is governed by the dissolution rates of the oxide film formed on chromium-depleted regions along the grain boundaries and of the metal matrix through defects in the oxide film.

5.2 SCC of High Nickel Alloys

Nickel base alloys, such as Alloy 600, and the high nickel, iron base Alloy 800 have been used for steam generator tubes of most LWRs and have so far suffered from various kinds of environmental degradation such as SCC, denting and intergranular attack (IGA). These alloys are still not necessarily free from corrosion problems. NRIM has been strongly interested in the corrosion problems of nickel base alloys and has performed studies of environmental degradation of these alloys in a similar manner to the corrosion problems of austenitic stainless steels in LWR coolant environments. Fig. 12[16] shows that the SCC of Alloy 600 is accelerated in acidic solutions, in which the post heat treated specimens were more susceptible to SCC than solution treated specimens. In the study of heat treatment effect[17], it was shown that the SCC susceptibility of Alloy 600 in high temperature acidic solutions increased with degree of sensitization measured by EPR (Electrochemical Potentiokinetic Reactivation) tests. The general trends for the SCC of Alloy 600 in acidic solutions were similar to those for austenitic stainless steels in terms of the following points: 1) in high temperature water containing chloride ions, annealed materials show transgranular cracking, while post heat treated materials show intergranular cracking with a high susceptibility for SCC, 2) crevices

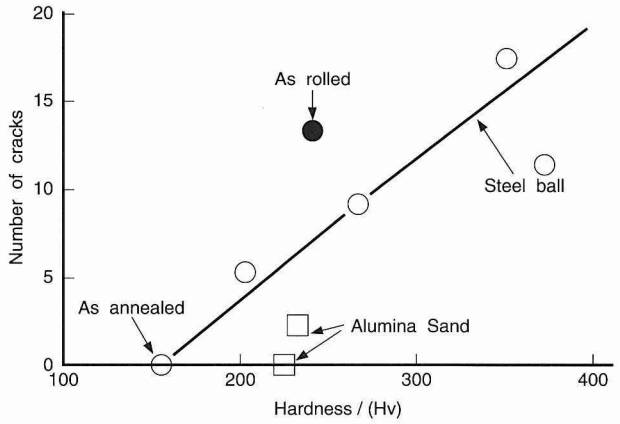

Fig. 14 Relation between number of small cracks and hardness of shot-peened Alloy 800 in boiling 50%NaOH + 0.3%SiO_2 solution

and high DO concentrations accelerate SCC, and 3) a temperature region (553~573 K) exists that shows a maximum SCC susceptibility. Fig. 13[16] summarizes the effects of DO, pH and crevices on the SCC susceptibility of Alloy 600. The figure shows no cracking in the dilute alkaline region, although there appears to be a region in which alkaline cracking would be expected in concentrated alkaline solutions. However, the cracking mechanism of Alloy 600 in alkaline solutions is considered to be different from that of austenitic stainless steels in high temperature water.

Shot-peening is expected to be effective for the mitigation of SCC and has been applied to SG tubes in some PWR plants in Germany and China. NRIM conducted a cooperative research program with an institute in China to determine the effect of shot peening on the SCC behavior of Alloy 800. The results of SCC tests using double U-bend specimens in boiling 50%NaOH + 0.3%SiO_2 solution and using C-ring and double-U bend specimens in 10%NaOH solution at 593 K were that the SCC susceptibility of Alloy 800 increased with the addition of shot peening. This was considered to be due to the effect of work hardening on the specimen surface by shot peening, which can increase the flow stress of the shot-peened layer above that of untreated specimens. Shot peened specimens that retained residual compressive stress on the surface showed less susceptibility than cold rolled specimens with the same surface hardness, as shown in Fig. 14[18]. This figure shows the effect of hardness on the number of small cracks observed after

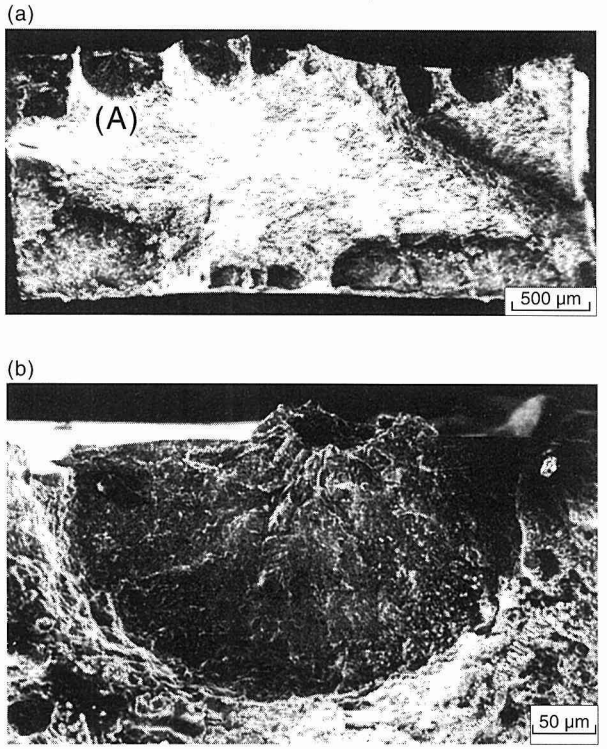

Fig. 15 A fracture surface of STS 42 carbon steel tested in 8 ppm DO water at 523 K. (Note that a crack starts from the pit (b).) Strain rate: 4.2×10^{-6} s^{-1}

boiling in an alkaline solution. Specimens blasted by alumina sand showed less susceptibility than those blasted by steel balls. In conclusion, shot peening treatments can be effective if the compressive stress due to shot peening reduces the residual tensile stress or if the component is used under low applied stress; otherwise, surface work hardening raises the applied flow stress, reducing the effect of the residual compressive stress.

5.3 SCC of Carbon Steels

It is well known that carbon and low alloy steels have excellent SCC resistance. These steels have been used in applications such as secondary recirculation piping and pressure vessels, and no SCC failures have been reported for LWR components made from carbon steels. It has been demonstrated, however, that carbon steels show SCC susceptibility when exposed in accelerated laboratory tests[19–21]. A typical example of SCC of carbon steel is shown in Fig. 15[21], which was obtained by SSRT in high temperature water with 8 ppm DO. NRIM confirmed that SCC tends to occur at the bottom of corrosion

Table 3 Results of SCC tests for STPT 42 carbon steel in high temperature water

Test conditions	Time to failure (h)	Cycles (N)	Strain (%)	Strain rate × 10^{-6}/s	Crack propagation rate × 10^{-10}m/s
(a)	3, 639 NF*	–	–	–	–
(b)	3, 010 NF*	378	2.8	1.3	–
(c)	3, 062 NF*	1, 020	0.7	0.6	–
(d)	1, 041 Leak	130	4.8	2.2	4.0
(e)	630 Break	79	5.0	2.3	13.2
"	930 Break	116	4.9	2.3	9.0
(e')**	10, 027 NF*	1, 253	3.4	1.6	–
(f)	589 Leak	147	2.9	2.7	7.1
(g)	528 Leak	132	3.5	3.2	15.8
(h)	2, 911 Leak	243	3.7	2.1	4.9

* No failure
** DO 0.2 ppm

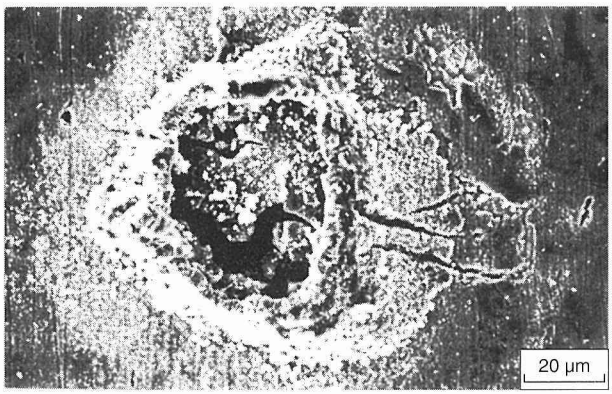

Fig. 16 Corrosion pit formed on STS 42 carbon steel tested in 8 ppm DO water at 523 K. (Note small cracks across the pit.) Strain rate: 4.2 × 10^{-6} s^{-1}

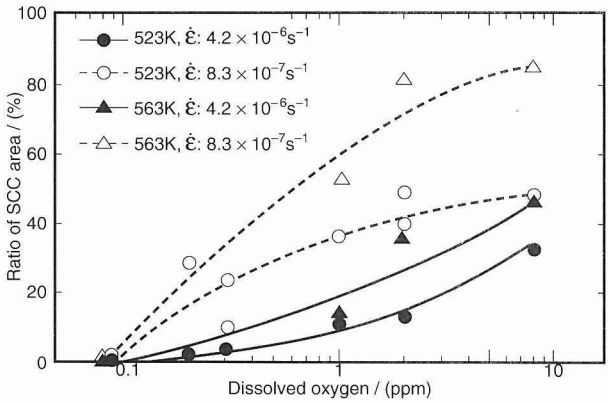

Fig. 17 Ratio of SCC area as a function of DO concentration for STS 42 carbon steel tested in water at 523 K and 563 K. Strain rate: 4.2 × 10^{-6} s^{-1} and 8.3 × 10^{-7} s^{-1}

pits originating from the dissolution of MnS inclusions in the manner illustrated in Fig. 16[21]. Reductions of DO concentrations in high temperature water decrease the occurrence of SCC in carbon steel, and no SCC was observed below 0.1 ppm DO, as shown in Fig. 17[21]. Since a potential-pH diagram for the Fe-H_2O system at 563 K indicates that the Fe_3O_4/Fe_2O_3 redox potential is attained around 0.1 ppm DO, it can be assumed that, above 0.2 ppm DO, magnetite is partially oxidized to hematite, forming a double-layered oxide film. The hematite layer in this film increases in thickness with increasing DO concentration, and the double-layered oxide film becomes more likely to produce corrosion pits for crack initiation.

NRIM has performed SCC tests under bi-axial loading by using tubular specimens to simulate small schedule piping in power plants during start-up and shut-down periods. Thus, fluctuations of the water temperature and stress were identified as factors accelerating the SCC of carbon steel. The specimen dimensions and the test apparatus were presented in Figs. 4(a) and 2, respectively. Fig. 18[22] is a schematic illustration of the water temperature and stress waveform used for the SCC tests. The results of the SCC tests on carbon steel are summarized in Table 3[22]. The table shows that the occurrence of SCC depends on the level of strain rather than the strain rate, and that the crack growth rate increases with increasing strain. It was confirmed that SCC also initiates at corrosion pits on the inner surface of the specimen, similar to the case of stainless steels.

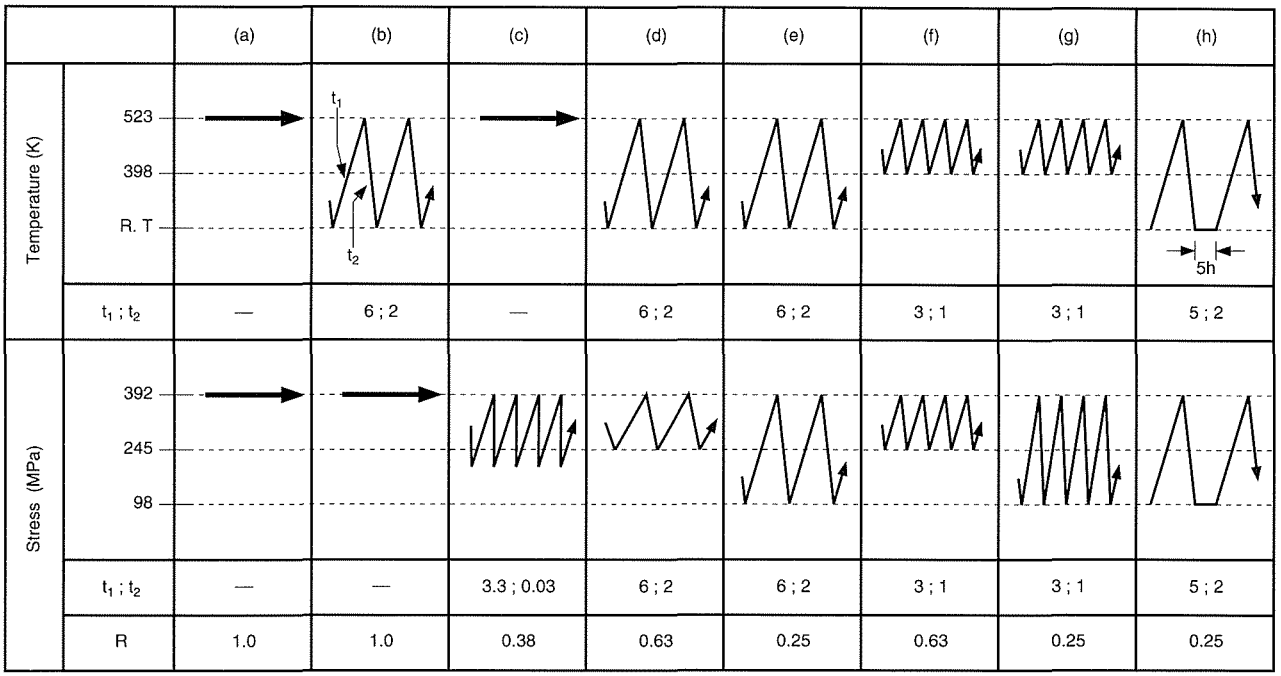

Fig. 18 Schematic illustration of waveforms of water temperature and stress used for SCC tests

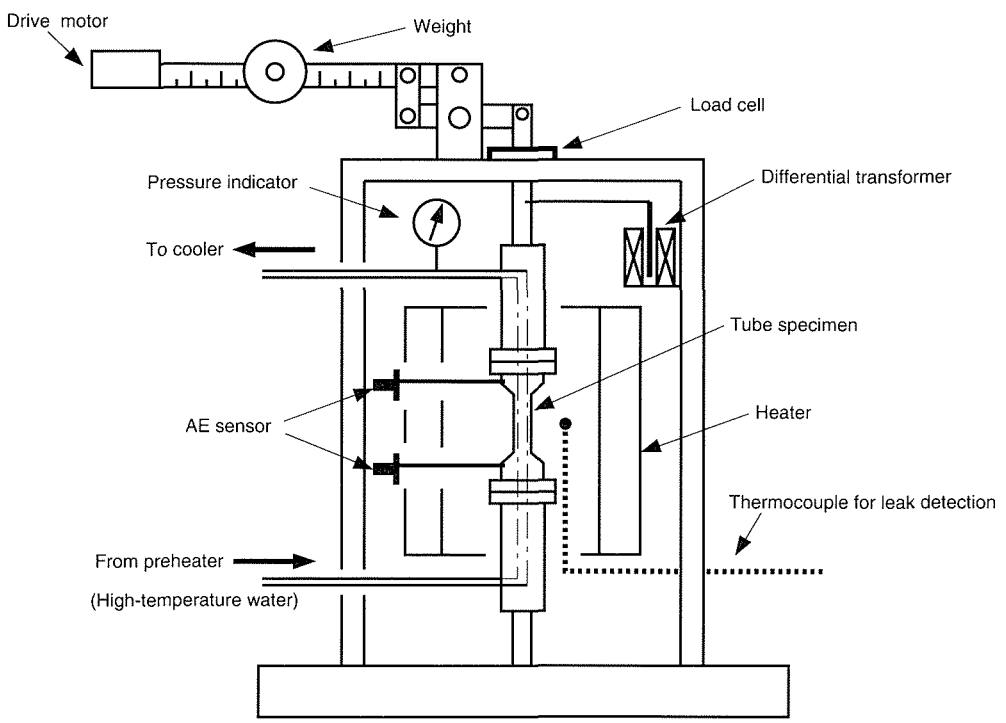

Fig. 19 Schematic diagram of an apparatus for AE measurement in SCC test using tubular specimen

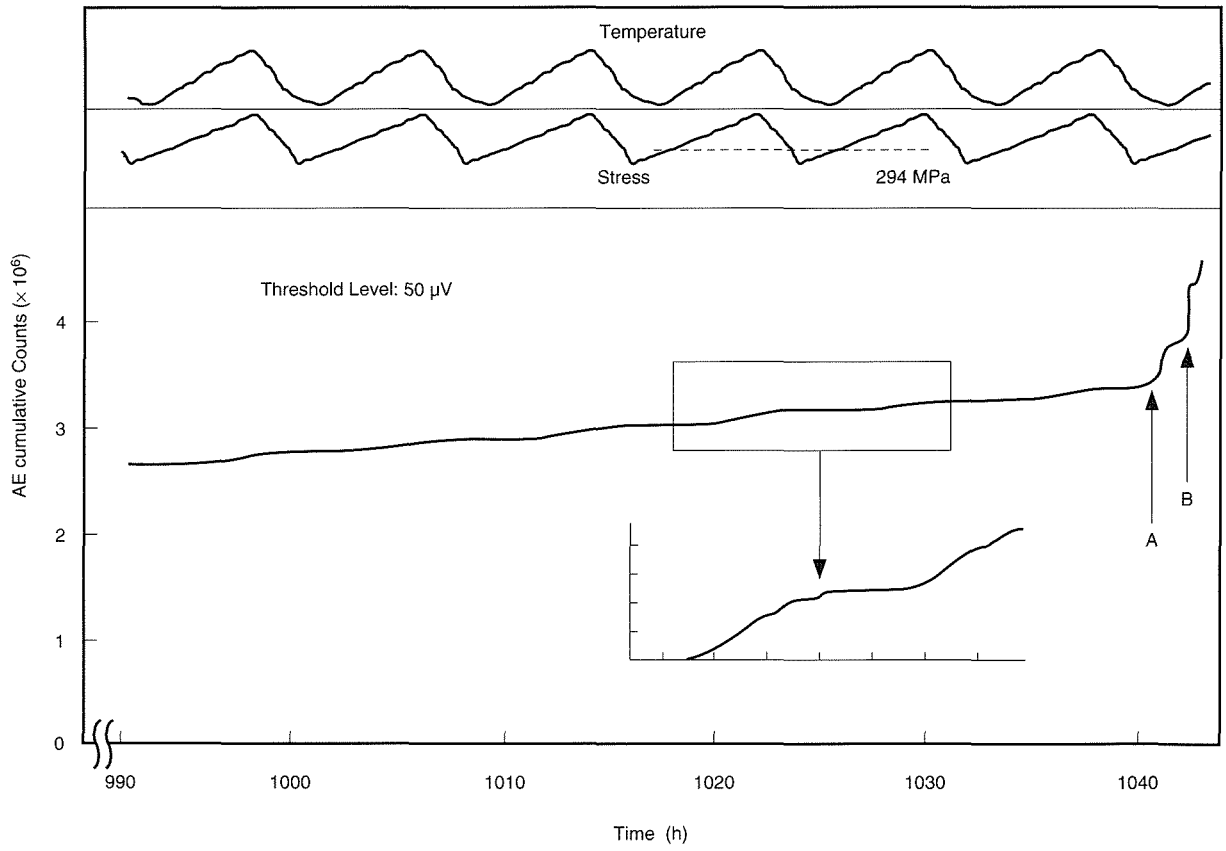

Fig. 20 AE cumulative count during SCC progress under the test condition of Fig. 18(d)

The applicability of acoustic emission (AE) was also investigated during this program because it was expected to be a useful tool for the detection of SCC propagation. AE signals were detected by a couple of AE sensors through transmission bars that were welded to the tubular specimen, as shown in Fig. 19[22]. Fig. 20[22] shows changes in the AE cumulative count with time. The cumulative number of AE events clearly increases rapidly at point "A" prior to water leakage at point "B", suggesting that AE can be a reliable monitor of SCC propagation. It was found that the propagation rate of SCC in carbon steel was one order of magnitude lower than that of 304 stainless steel, possibly due to the branching of cracks.

The minimum time to failure was obtained at condition (e) in Fig. 18, where the specimen was separated by circumferential failure. However, no failures were observed after more than 10^4 h when the DO concentration was reduced to 0.2 ppm, which corresponds to the DO levels of BWRs. It was observed that at low DO levels, a stable black oxide film formed without any corrosion pitting. This implies that the selective dissolution of inclusions might be suppressed by a dense oxide film.

6. CF of Low Alloy Steels

6.1 Low Cycle Fatigue

For designing structural components that will be subjected to cyclic loads, the fatigue behavior of the materials to be used must be clarified and their design fatigue curves established in advance. When the material is used in corrosive environments, further investigations are needed because the fatigue behavior of the material is influenced by the environment. Pressure boundary components of LWRs, such as the pressure vessel and the primary coolant piping system, require superior integrity throughout their lives and are designed using the design fatigue curves specified in Section III of the ASME Boiler and Pressure Vessel Code[23]. These design fatigue

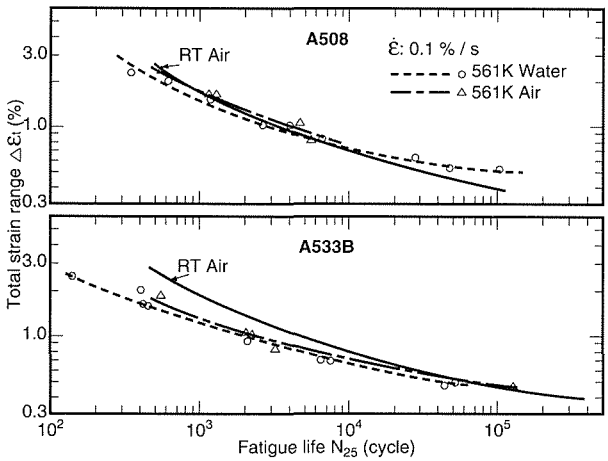

Fig. 21 S-N curves for low alloy steels in high temperature water and air

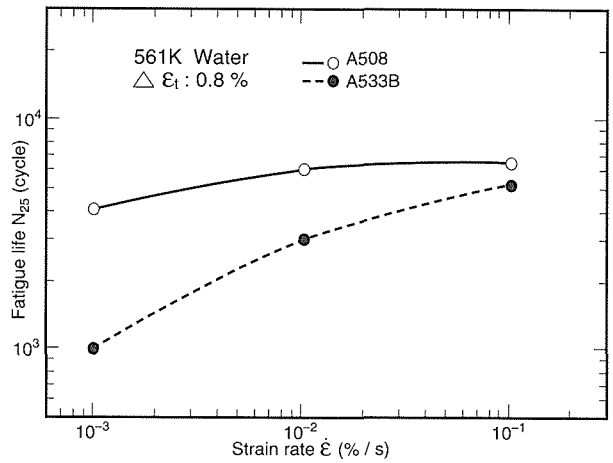

Fig. 22 Strain rate dependence of fatigue life for low alloy steels in high temperature water

curves were established on the basis of experimental S-N data obtained in ambient air and include safety margins for effects such as test specimen size and data scatter. However, the safety factor in the ASME Sec. III design fatigue curves against laboratory data is one twentieth in the number of cycles to failure or one half in fatigue strength. These curves do not include any factor for environment because the environment depends on the conditions of each specific application. Although the inner wall of the pressure vessel is covered with austenitic stainless steel cladding, its soundness is usually evaluated using the fatigue behavior of low alloy steel in an aqueous environment under the assumption of direct contact with the coolant[24-26]. Since the materials employed for pressure boundary components frequently show a reduction in fatigue life or an acceleration of the fatigue crack growth rate in a simulated reactor environment, it is important to clarify the extent of any environmental effects on the design fatigue curves of the ASME Code, as well as to establish databases that can be used with life prediction techniques.

6.1.1. Effect of high temperature water environment on S-N curves

Fig. 21[27, 28] shows a comparison of S-N curves in high temperature water, high temperature air and room temperature air at a strain rate of 0.1%/s. A533B steel shows a reduction of fatigue life in a high temperature water environment, especially at high total strain ranges, whereas the fatigue life of A508 in a high temperature water environment tends to extend that at low total strain ranges. The results for the A533B steel indicate that the effect of a high temperature water environment on fatigue consists of two components, a temperature effect and a water environment effect. However, the test temperature defines the shape of the S-N curve, and the water environment is not as influential as expected. It should be pointed out that a temperature effect, as well as a pure environmental effect, should be incorporated into the design fatigue curves in the ASME Code because the curves do not include the temperature effect either.

Strain rate is an influential factor in strain controlled fatigue tests. The strain rate dependence of S-N curves for steels is not large in ambient temperature. However, it is suspected that superposition of the environmental and strain rate effects might significantly affect the S-N behavior. Fig. 22[27] presents log-log plots of the strain rate dependence of fatigue life at the specific total strain calculated from the S-N curves for A508 and A533B steels[27, 28] at strain ranges from 10^{-1}%/s to 10^{-3}%/s in high temperature water. The curves may be postulated as linear, as expressed by:

$$N_{25} = C\dot{\varepsilon}^{\gamma} \quad \cdots\cdots (1)$$

where $\dot{\varepsilon}$ is strain rate. The value of γ is 0.10 for A508 and 0.36 for A533B. Since contradictory results have been reported[29], this kind of behavior seems to be influenced

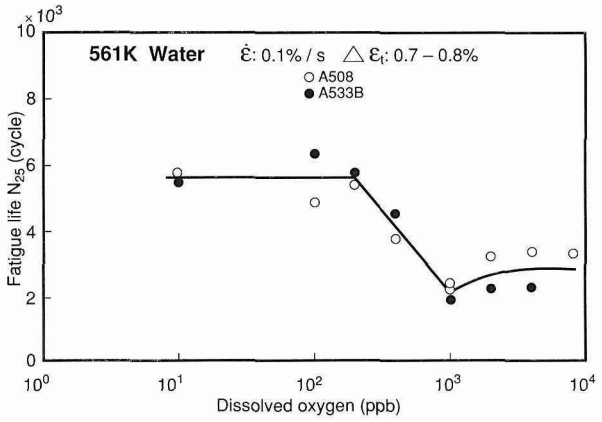

Fig. 23 DO concentration dependence of fatigue life for low alloy steels in high temperature water

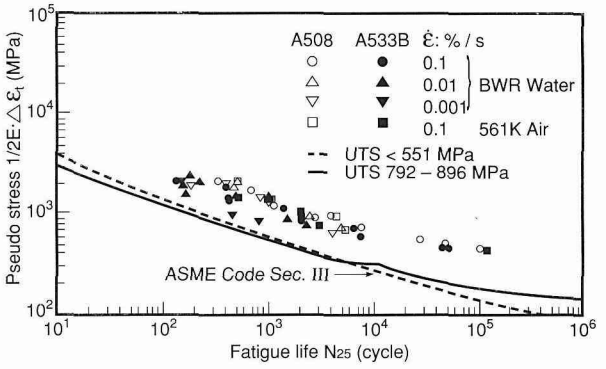

Fig. 24 Comparison of the present data with the design fatigue curves in the ASME Code, Sec. III

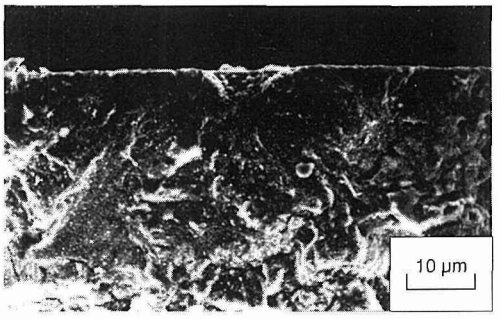

Fig. 25 A typical example of fatigue crack initiation on the fracture surface of A533B steel in high temperature water

by metallurgical factors rather than steel type. Occasionally, actual conditions are not evident from laboratory tests, and longer duration tests are needed. Since the loading rate for actual reactor components is probably much lower than those used in the present tests, the acquisition of data at extremely low strain rates is considered to be urgent, although this kind of test is quite time consuming. One report[30] indicates that the strong strain rate dependence of carbon steel in BWR water environments tends to diminish at strain rates lower than 10^{-4}%/s. This conclusion suggests that there is some limit to the reduction of fatigue strength due to strain rate effects in high temperature water environments, and that further, long-duration investigations should be recommended.

The DO concentration dependence of both steels shows a complex behavior, as shown in Fig. 23[27, 28]. Contrary to the strain rate dependence seen in Fig. 22, there is no difference between A508 and A533B steels. The transition behavior of the fatigue life between 200 ppb and 1000 ppb in Fig. 23 was also reported for low alloy and carbon steels[31].

6.1.2. Comparison with ASME Code, Sec. III

Design fatigue curves for nuclear reactor components are given in the ASME Boiler & Pressure Vessel Code, Section III[23]. These curves are developed from the minimum of either half the stress or one twentieth the fatigue life of the best fit curves of fatigue data obtained in ambient air, taking into account of the effects of test specimen size, data scatter and other variables, but not environmental effects. For the application of these curves to components used in other environments, the use of factors for environmental effects is necessary. Fig. 24[27, 28] is a comparison of current fatigue life data with the ASME design fatigue curves, expressed as a pseudo-stress. All of the fatigue data obtained in high temperature water falls above the design fatigue curves with margins of twice the stress or ten times the fatigue life. However, since the materials employed show a clear strain rate dependence in high temperature water environments, as discussed in the previous section, a lower margin is expected for data points at lower strain rates than those tested. These results may instigate a revision of the design fatigue curves that takes environmental effects as well as the strain rate effect into account.

6.1.3. Origin of fatigue cracking in high temperature water

Fractography of fractured surfaces indicates that the fatigue cracks initiate from corrosion pits on the surface

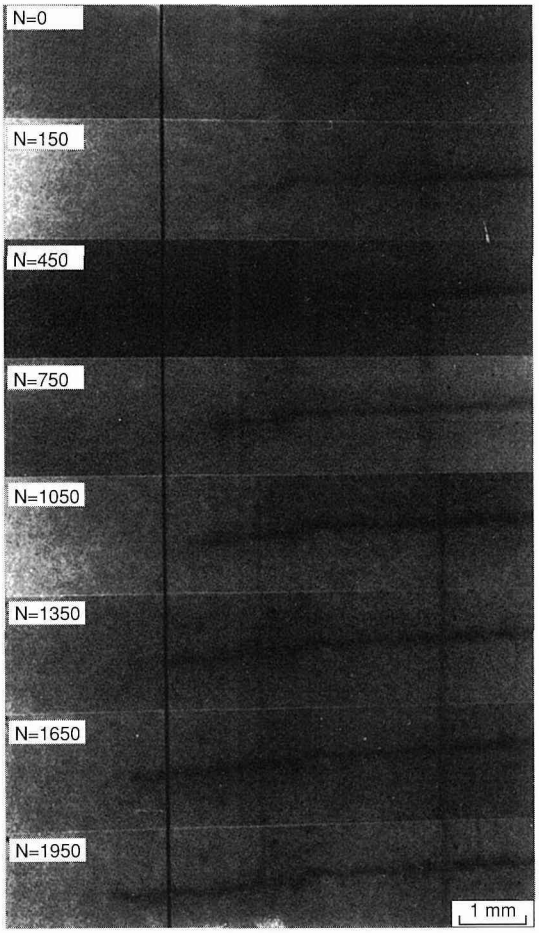

Fig. 26 Successive observations of fatigue crack growth in water at 561 K

that are formed by dissolution of the MnS inclusions, as shown in Fig. 25[27]. Correlation of the dissolution of MnS inclusions with the formation of corrosion pits has been confirmed by successive observations of MnS dissolution behavior. Investigation of the surfaces and sections of fatigued specimens revealed that the fatigue cracks initiate from the bottom of corrosion pits. In addition, investigation of the surface corrosion behavior of the steels revealed a correlation between the corrosion pit density and the sulfur content. It can be concluded from these investigations that the fatigue crack initiation mechanism for these steels in high temperature water is such that corrosion pits are generated by dissolution of MnS inclusions on the surface that act as points of stress concentration for the origins of cracking. The early formation of corrosion pits due to high rates of dissolution of MnS inclusions provides points of stress concentration that precede the formation of intrusion sites and that reduce the number of cycles necessary for crack initiation, resulting in a reduction of the fatigue life. Even though the surface with corrosion pits was covered with a thick oxide film, the film might not affect this mechanism, because oxide film formed in the high temperature water consists of an aggregation of fine crystalline magnetite. Acceleration of crack growth rates due to a corrosive environment also contributes to a reduction in fatigue life. However, this appears to be minor from the present results because the crack growth behavior of steels containing sulfur below 0.010 wt% is considered to be nearly independent of the sulfur content[32, 33]. This may imply that the crack initiation process in high temperature water is more sensitive to the steel sulfur content than the crack growth process.

6.2 Fatigue Crack Growth

Crack growth behavior of structural materials, especially low alloy steels used for RPV in reactor coolants, has attracted world-wide attention since JAERI discovered the EAC behavior of ferritic steels in 1972[3, 4]. NRIM joined this complex research field in 1980 and has obtained extensive interesting knowledge, as outlined below.

6.2.1. Direct observation of cracking in high temperature water

In fatigue crack growth tests using common test pieces such as compact tension (CT) and center cracked tension (CCT) specimens, crack length is usually determined by either direct measurements of the crack, using a microscope or measuring beach marks on the fracture surface, or indirect measurements, using elastic compliance of the ligament or the electro-potential drop across the cracked ligament. However, crack length measurements for corrosion fatigue tests have so far been conducted exclusively by indirect methods because the specimen is inside of a high-pressure autoclave. The results of these indirect measurement methods have not yet been verified by optical measurements because of the technical difficulty. The technical problems remaining include finding a window material that is suitable as a pressure boundary for high temperature water, distortion of the image by thermal fluctuations in the water, and the

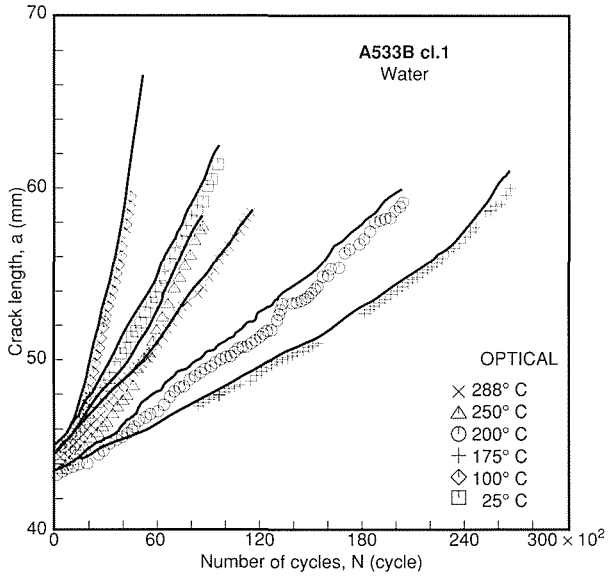

Fig. 27 Comparison of crack lengths measured by the optical observation method (symbols) and the compliance method (solid lines)

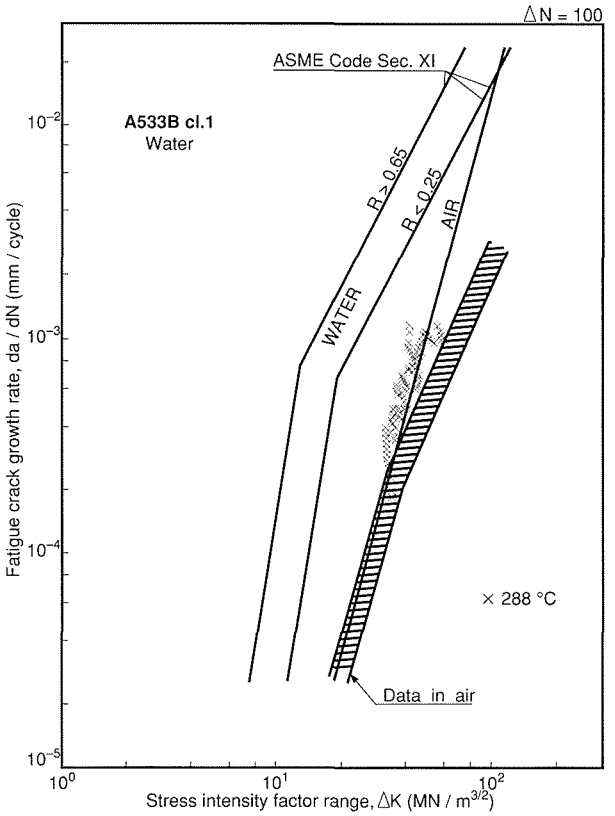

Fig. 28 da/dN-ΔK relationship for low sulfur A533B steel in water at 561 K

long working distances for a telescope due to the thick walls of the autoclave and mantle heater. The only report of direct observations is the work done by Kawakubo et al.[34] in which continuous optical observations of stress corrosion cracking in austenitic stainless steel in high temperature water at 523 K were carried out using single crystal sapphire glasses and a TV camera. The author was very encouraged by their techniques and designed a direct observation system for corrosion fatigue tests, which was introduced in Section 4. The key to the direct observation technique was to use a long, transparent single crystal sapphire rod as a solid image path in the high temperature water. The sapphire rods were produced by Toshiba Ceramics Co. An autoclave with extended window ports and a specially-designed observation system was constructed (Fig. 3(a)). It was found that the observation system possessed a resolution of 0.01 mm, which satisfied the ASTM Standard E647 requirement for fatigue crack measurements. Fig. 26[35] is a partial set of successive observations of a fatigue crack in water at 561 K. Fig. 27 [35] is a comparison of crack lengths measured by the optical observation and compliance methods. The present compliance method employed a LVDT (linear variable differential transformer) designed for high temperature water. This is the first comparison of the two methods that verifies a good correlation. The trend that all crack lengths measured by the optical method are slightly smaller than those measured by the compliance method is due to the so-called tunneling effect of fatigue crack fronts. Direct observations sometimes provided a variety of information on crack growth behavior, such as branching and detouring of the crack path.

6.2.2. Effects of variables on fatigue crack growth rates

As mentioned in Section 3, NRIM studied the effects of environment on the fatigue crack growth behavior of low alloy steels in simulated LWR coolant environments. This section introduces these effects in addition to presenting the effect of some mechanical and metallurgical factors.

Basic da/dN-ΔK relation

Reference curves for the crack growth rates of ferritic steels in reactor coolant environments are presented in

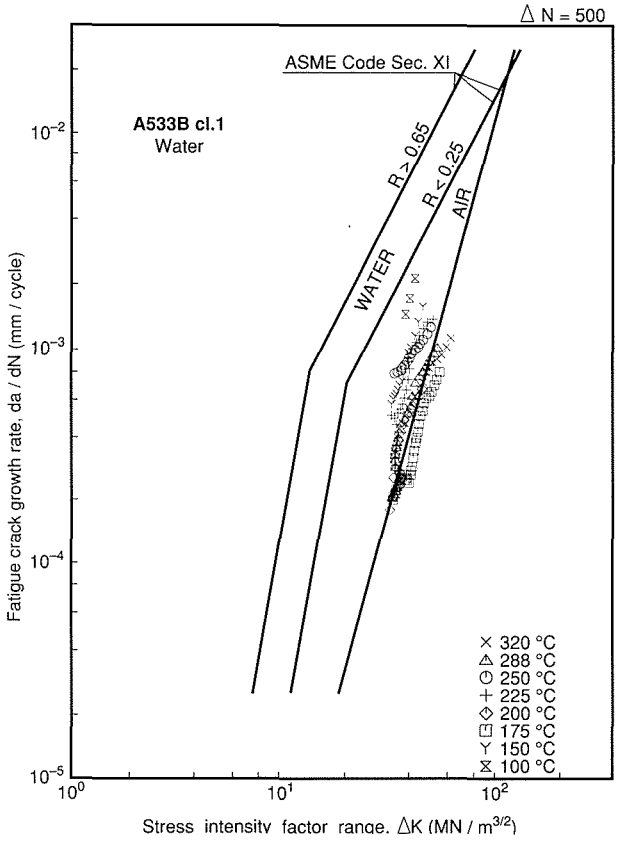

Fig. 29 da/dN-ΔK relationships for low sulfur A533B steel in water at various temperatures

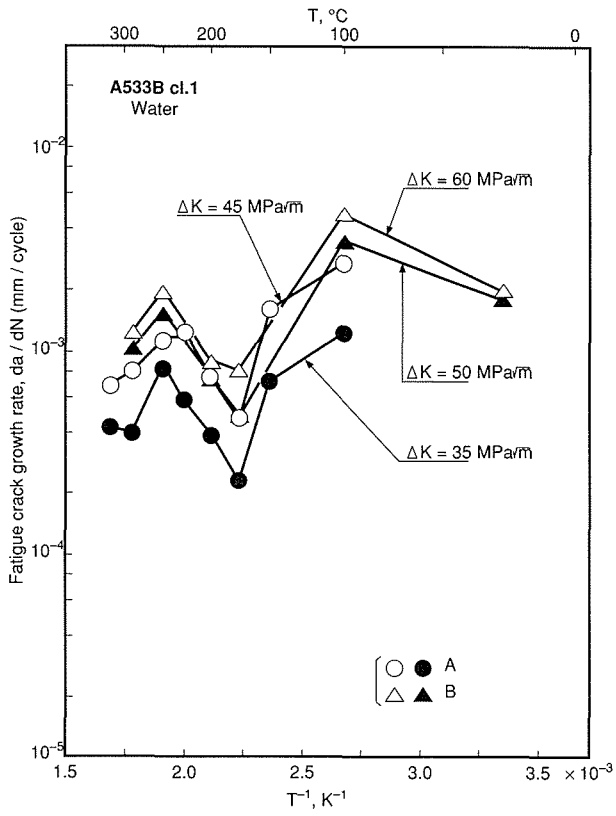

Fig. 30 Temperature dependence of fatigue crack growth rate for A533B steel in simulated BWR water environment

ASME Code Sec. XI, which is an inspection code for reactor components. Typical examples of data following the ASME Code for low alloy steels in a simulated BWR coolant environment are shown in Fig. 28[36]. Although data points obtained from high temperature water tests are scattered around the air curve of the ASME Code, some acceleration is clearly observed when compared to the ambient air data of the material used. The data points are limited because of the experimental difficulty and the data reduction process. EAC tests consist of time-consuming, low cycle loading, and there is a limit to data acquisition for low crack growth rates around K_{th}. Data reduction using the seven point polynomial analysis method also cuts out data points at the start and end of the test, especially for large acquisition intervals. These are reasons why very few crack growth curves have been obtained at K_{th}.

Effect of temperature

Materials experience various temperatures depending on the reactor component application and the effect of start-up and shut-down operations. Fig. 29[36, 37] shows the effect of temperature on the crack growth rate of A533B steel in pure water containing a DO concentration of 100 ppb. The sampling interval was set at 500 cycles to avoid a large scatter of data at the initial stage of the fatigue tests. The crack growth rate varies widely, and the maximum effect is observed at 373 K. The temperature dependence at different ΔK values is shown in Fig. 30[36, 37]. These have very complex shapes, suggesting multiple controlling mechanisms. Similar results have been reported for experiments in BWR and PWR water environments[38–40]. Fig. 27 includes data from specimens with sizes that vary by a factor of four and suggests that there is no specimen size effect on crack growth rate. Care must be taken to consider the result at 373 K, for which the data points are close to the ASME reference curve for low ΔK, even though the material is classified as a low sulfur material. This curve is the highest of those obtained under conditions that nuclear power plants experience through their operations. The temperature

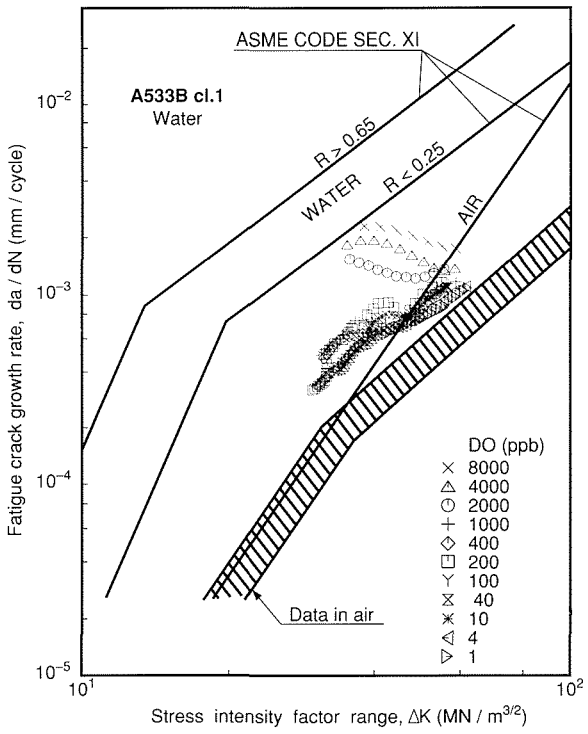

Fig. 31 da/dN-ΔK relationships for low sulfur A533B steel in high temperature water containing various DO concentrations

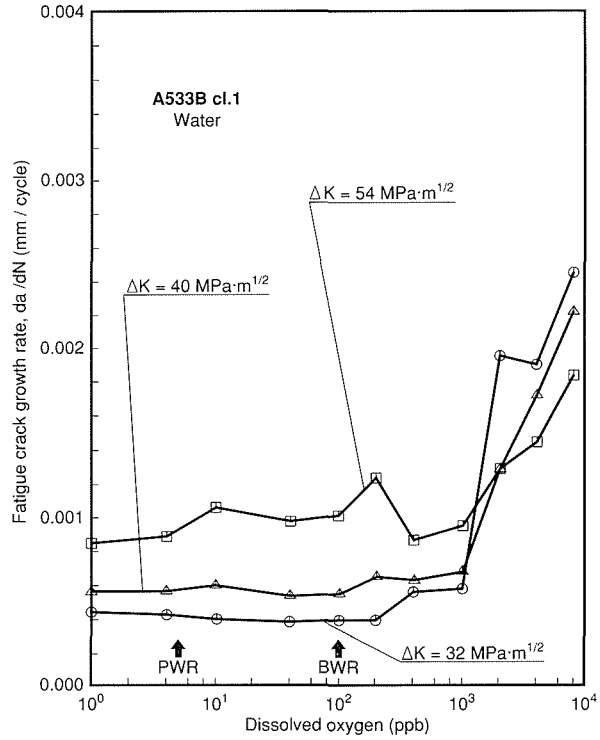

Fig. 32 DO concentration dependence of da/dN for low sulfur A533B steel in water at 561K

effect appears to be one of the factors to be discussed when the reference curves are modified.

Effect of dissolved oxygen

Dissolved oxygen is an important influential factor for materials in high temperature water. It occasionally accelerates damage of the material, such as with corrosion fatigue and stress corrosion cracking, not to mention general corrosion. NRIM investigated the effect of dissolved oxygen concentration on the crack growth rate of A533B steel in water at 561 K. The oxygen concentration of water in a make-up tank of the recirculation system was controlled from a saturated concentration at room temperature to 1 ppb. Fig. 31[37, 41] shows the relation between fatigue crack growth rate and stress intensity factor range at various DO concentrations in water at 561 K. It is clearly seen that dissolved oxygen concentrations above 1000 ppb in high temperature water accelerate the crack growth rate of the material, especially at low ΔK values. The rate of acceleration has a maximum factor of 3 at DO concentrations below 1000 ppb, while above 1000 ppb the factor reaches 8. The DO concentration dependence of the crack growth rate is shown in Fig. 32[41], in which crack growth rates at specific values of ΔK are replotted against a logarithmic DO concentration scale. It is seen that the crack growth rate scarcely depends on DO concentration below 1000 ppb, implying a similarity in the degree of EAC damage between the coolant conditions for BWR and PWR. The reverse trend of the crack growth rate, i.e. decreasing with increasing ΔK at DO concentrations above 1000 ppb as shown in Figs. 31 and 32, is considered to be due to a decrease in the effective ΔK caused by an oxide-induced crack closure effect.

Electrochemistry is a strong tool for understanding the behavior of materials in solutions associated with corrosion. The polarization curves and corrosion potentials of A533B steel were obtained after overcoming technical difficulties with the high temperature water environment. Fig. 33[41] is a comparison of corrosion potentials from the present work with those from the literature[33]. The corrosion potential increases with increasing DO concentration and shows good consistency with the literature. The relation between the fatigue crack growth rate and DO concentration in Fig. 32 is associated

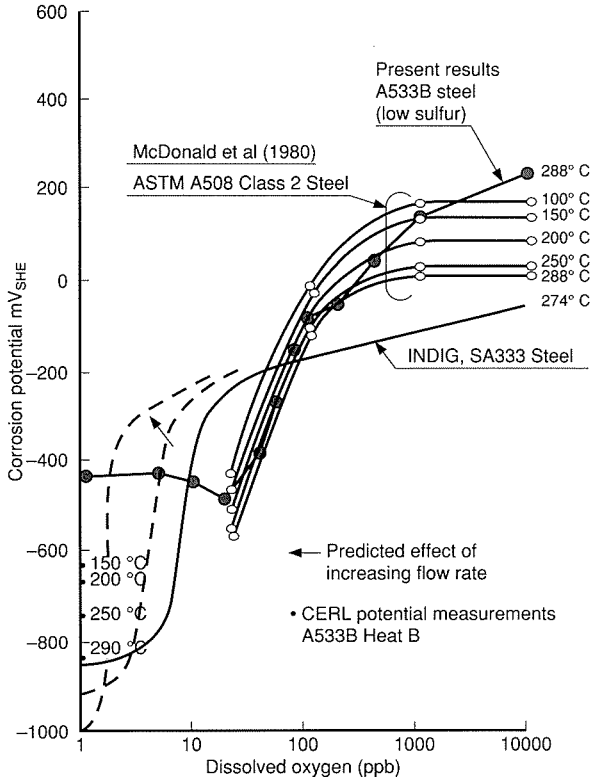

Fig. 33 Comparison of the present results of corrosion potential with the literature[42]

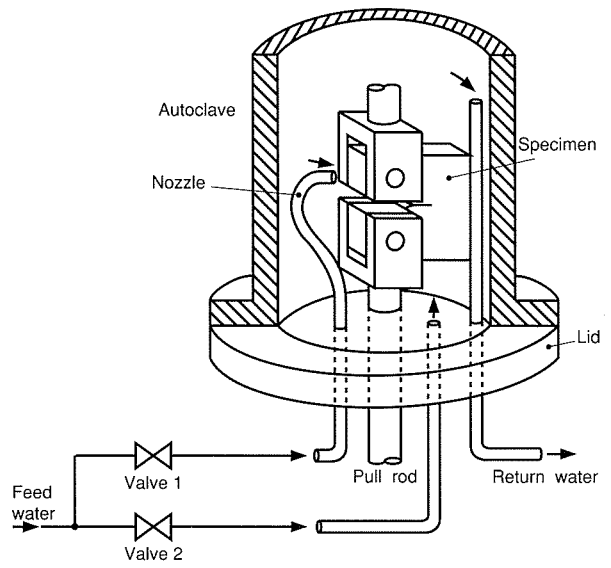

Fig. 34 Schematic diagram for an apparatus for water flow rate change tests

with local corrosion, while that between the corrosion potential and DO concentration in Fig. 33 is associated with general corrosion. Therefore, a strict comparison of the two phenomena may not be reasonable. However, a qualitative discussion of the relation between Figs. 32 and 33 from the electro-chemical viewpoint may be as follows. The cathodic reaction in the system was activated by the high DO concentration, so that the measured corrosion potential has shifted to a more noble potential from the equilibrium potential of the system. On the other hand, fresh metal surface associated with fatigue crack growth dissolves rapidly with increasing DO concentration, especially at DO levels higher than 1000 ppb. This results in acceleration of the crack growth rate. Acceleration of the crack growth rate might correspond to the transpassive region of the anodic polarization curves of the material.

Effect of flow rate

The average flow rate of laboratory water recirculation systems is commonly much less than those of nuclear power plants, and expensive pump systems are required to simulate the effect of high water flows. UKAEA Risley installed a recirculation system with a high flow pump and published an EAC map for low alloy steels in terms of the flow rate and sulfur content[42]. The author designed a device for changing the water flow rate by putting a nozzle in front of the specimen crack mouth, as shown in Fig. 34[43]. The nozzle can feed a water jet directly into the crack mouth. The flow rate can be changed through the nozzle or the inlet hole of the lid in addition to varying the pump speed of the recirculation system. It was found that A533B steels with differing sulfur contents had lower crack growth rates at high flow rates with the nozzle than those under low flow rates without nozzle, as shown in Fig. 35[43]. The curves also show the effect of sulfur content. A medium sulfur steel (containing 0.014 wt%S) had a drastic change in the crack growth rate compared to that of the low sulfur steel (0.004 wt%S). We can conclude from these results that sulfur strongly influences the fatigue crack growth behavior of ferritic steels in high temperature water, especially under stagnant conditions.

Another finding of corrosion fatigue behavior from using the flow rate change tests is that fatigue crack growth responds promptly to changes in the flow rate, as shown in Fig. 36[43], in which the corrosion potential

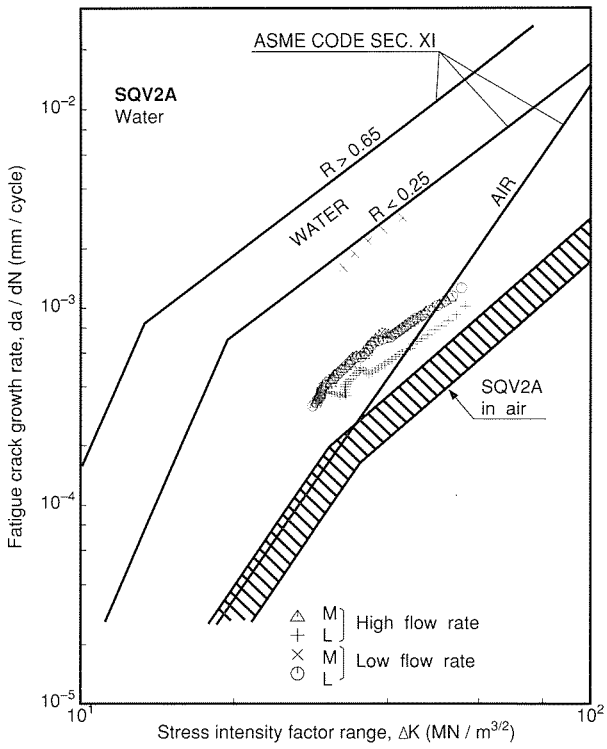

Fig. 35 Effects of water flow rate and sulfur content on da/dN-ΔK curves for A533B steels

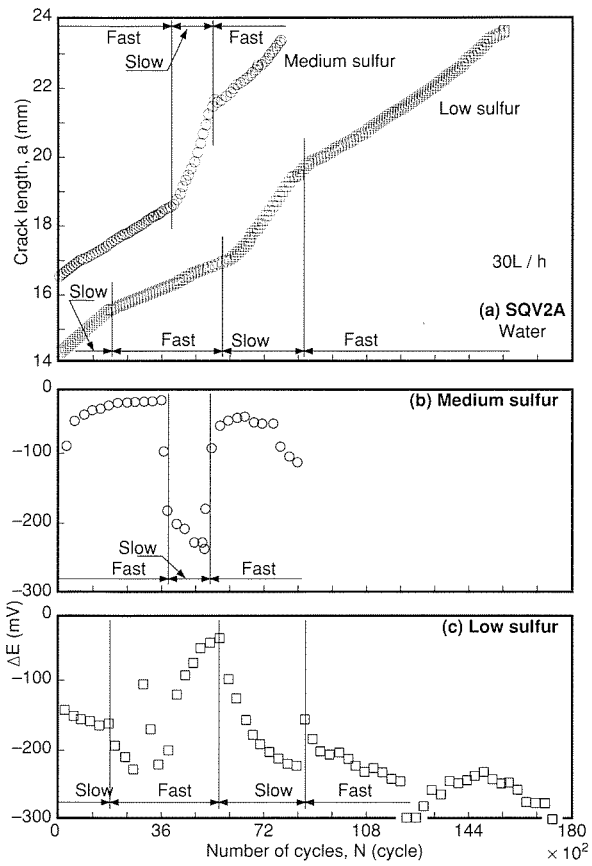

Fig. 36 Effects of water flow rate on crack length vs N curves (a) and corrosion potential (b) (c) for A533B steels

response is also shown. In this case, changes of the crack growth rate and corrosion potential due to the flow rate were again enhanced for the medium sulfur steel. This result also indicates the strong effect of sulfur on the EAC behavior of steels.

The flow rate dependence of the normalized crack growth rate is summarized in Fig. 37[43] for both steels. In this figure, the ordinate represents an EAC enhancement factor expressed as:

$$A^{*} = (da/dN)_{water} / (da/dN)_{air} \quad \cdots\cdots\cdots\cdots\cdots \quad (2)$$

The ultimate value of A^{*}_{HIC} should include influential factors, such as the high stress ratio and low cyclic frequency, in addition to the present factors of high sulfur content, stagnant water flow, and limiting values of such phenomenon as stress corrosion cracking accompanied by hydrogen induced cracking. The EAC mechanism controlling the present results is thought to be as follows: Under a stagnant water flow, the composition of the water in front of the crack tip would be different from that of

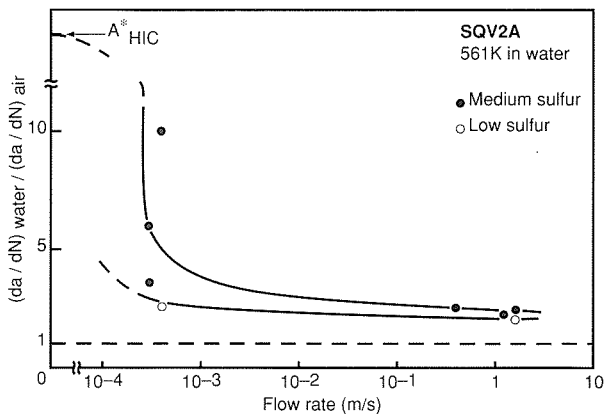

Fig. 37 Effect of water flow rate on environmental acceleration of crack growth in terms of da/dN

the bulk water. The DO concentration decreases with the consumption of oxygen during the formation of an oxide film on the bare metal surface, while the pH value drops

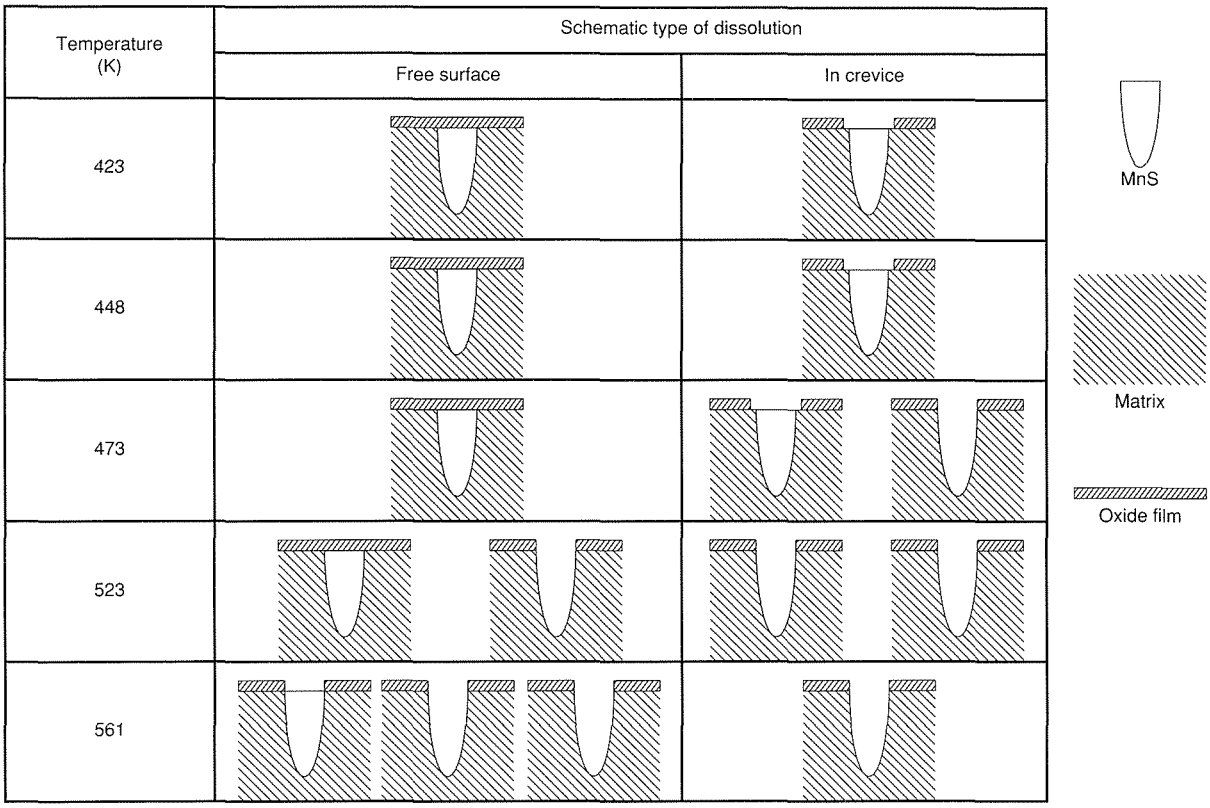

Fig. 38 Schematic illustration of the dissolution behavior of MnS

because dissolution of the bare metal produces hydrogen ions by the cathodic reaction. In addition, the dissolution of MnS inclusions also produces hydrogen ions at the crack tip. When the water jet is introduced to this condition, the anodic environment at the crack tip could be blown out and replaced by fresh test water with a high DO concentration. We conclude that EAC enhancement of the crack growth rate is governed by the low pH value rather than the high DO concentration by considering the DO concentration dependence shown in Fig. 31 which indicates that the crack growth rate does not vary with DO below 1000 ppb. The response of the corrosion potential in the water flow rate change tests shown in Fig. 35 can be explained by two points of view. One is the so-called differential aeration potential mechanism that is due to the reduction of the DO concentration at the crack tip at low flow rates. This mechanism seems to be reasonable qualitatively from the results of the relation between DO concentration and corrosion potential[33] and the measurement of DO concentration in the crack tip water[44]. The other reason is the dissolution of MnS inclusions and the decrease of pH by the cathodic reaction. Since the decrease of pH in the small gap has been recognized[45], the steep drop in the corrosion potential curve for the medium sulfur steel in Fig. 36 is attributed to active hydrogen ion generation by the cathodic reaction.

Corrosion behavior of MnS in relation to crack growth

In previous sections, we found that sulfur strongly influences the low cycle fatigue life and the fatigue crack growth rate of low alloy steels in high temperature, simulated LWR coolant environments. Sulfur is present as MnS inclusions in the matrix. When exposed to high temperature water, these inclusions dissolve through the following possible reaction:

$$MnS + 4H_2O \rightarrow Mn^{2+} + SO_4{}^{2-} + 8H^+ + 8e^- \quad (3)$$

This reaction results in a decrease of pH, which gives rise to hydrogen embrittlement at the crack tip[46]. MnS dis-

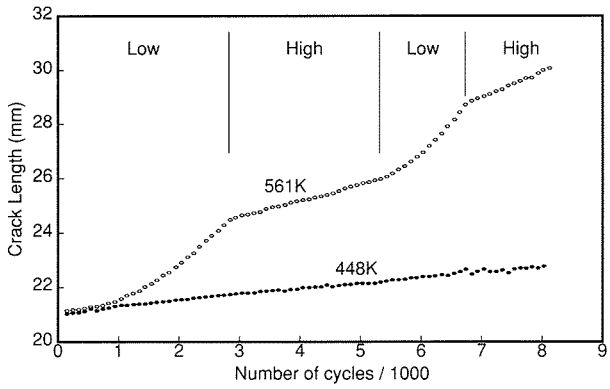

Fig. 39 Results of water flow rate change tests for medium sulfur A533B steel at different temperatures

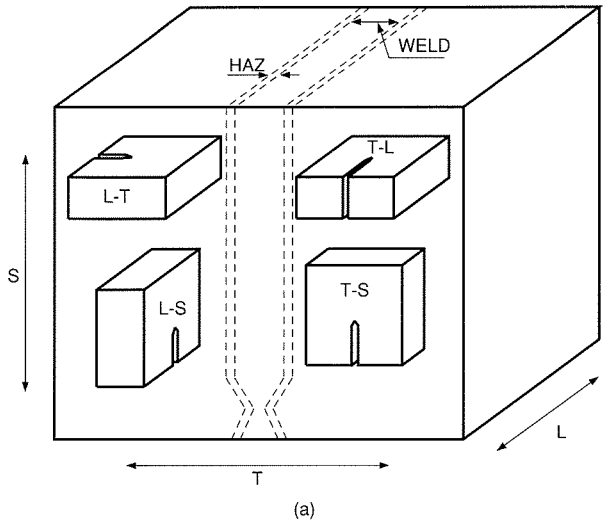

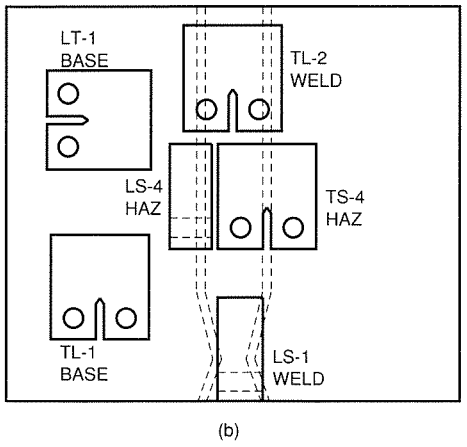

Fig. 40 Specimen notch orientations (a) and locations (b)

solves easily in high temperature water, forming a corrosion pit, which can act as a fatigue crack initiation site, or lowering the pH at a fatigue crack tip, which can accelerate the crack growth rate. Therefore, it is important to understand the dissolution behavior of MnS in a corrosive environment, especially at a crack tip in high temperature water. Pairs of coupons of medium sulfur A533B steel were pressed tightly together to simulate a crack gap and then immersed in water at temperatures ranging from 423 K to 561 K. This temperature interval includes the range of complex temperature dependence of crack growth rate shown in Fig. 30. The typical appearance of the specimen surface and a schematic illustration summarizing the MnS dissolution mechanism are shown in Fig. 38[47], respectively. It can be concluded from these results that MnS inclusions tend to dissolve in water above 448 K slightly easier in crevices than in the bulk condition. Differences between the BWR and PWR water chemistries did not result in any change. The former conclusion appears significant because it implies that MnS inclusions are not expected to influence the fatigue crack growth rate in water at temperatures below 448 K. This hypothesis was confirmed by the water flow rate change tests, as shown in Fig. 39[47]. In the figure, the curve at 448 K shows no kink due to flow rate change, which provides substantial evidence verifying the EAC mechanism in high temperature water.

Crack growth behavior of welded joints

The LWR pressure vessel is a large, welded structure composed of thick, low alloy steel. Noting the modifications in microstructure and the resulting increased defect density of welded parts, the evaluation of welded specimens must be of pragmatic importance. NRIM obtained 253 mm thick, wrought A508 steel, butt-welded joints in the same manner as the RPV components and examined the fatigue crack growth behavior of the different microstructures. CT specimens were cut from the welded joints to evaluate the effect of microstructure, such as in the weld metal and heat affected zone (HAZ), and the effect of microstructural orientation, as illustrated in Fig. 40[48]. Fig. 41[48] is a comparison of the crack growth curves of these specimens presented as in previous sections. The material demonstrated some acceleration due to EAC, while little difference was observed in regard to microstructure. There was no significant effect of residual stress

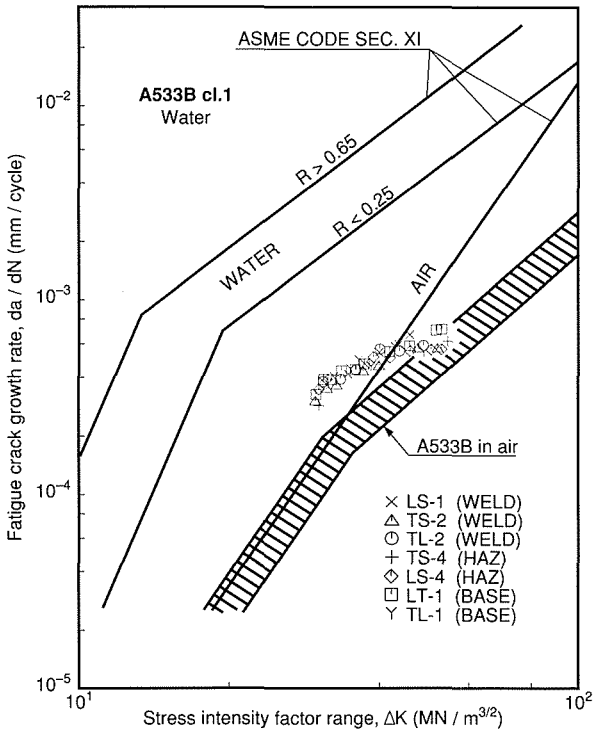

Fig. 41 da/dN-ΔK relationships for welded A508 steel

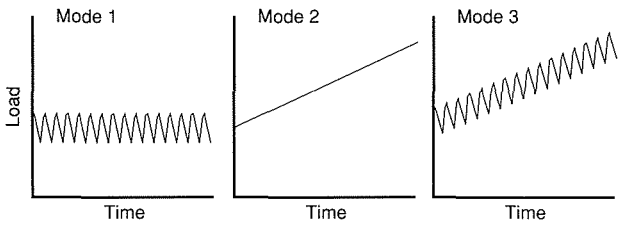

Fig. 42 Schematic illustration of loading modes for CF-SCC interaction

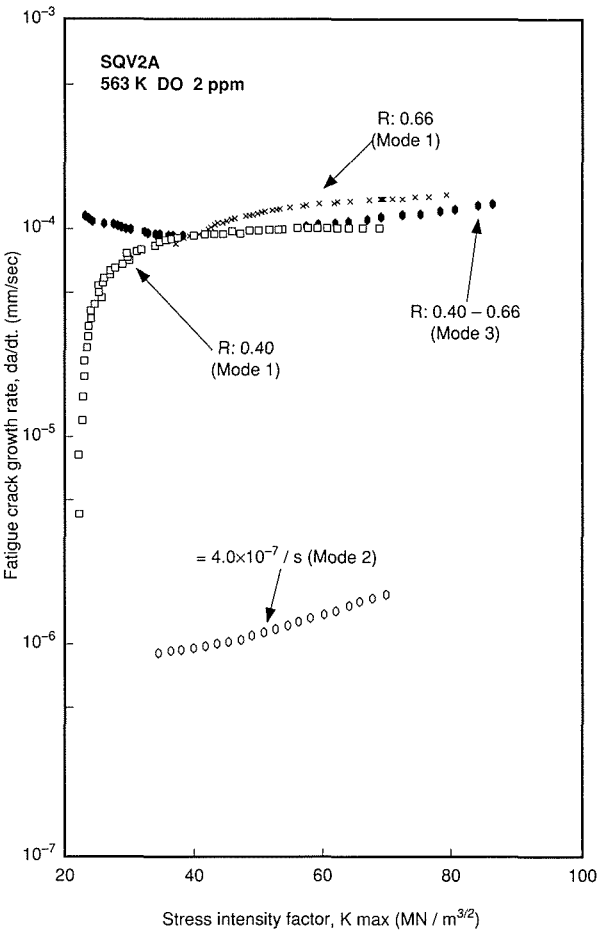

Fig. 43 da/dt-K_{max} relationships for A533B steel under loading modes shown in Fig. 42

of the weld joint, which was locally as high as 100–200 MPa, while the Vickers hardness number was about 20 higher for the weld metal than for the base metal. It is therefore concluded that the fatigue crack growth rate of welded joints may be represented by that of the base metal. The results also indicate that the domestic material used has a sufficient safety margin over the curves in the ASME Code Sec. XI.

6.3 Interaction of CF and SCC in Low Alloy Steel

NRIM was interested in establishing whether the interaction of CF and SCC could accelerate the crack growth of materials in high temperature water under actual loading conditions. Crack growth tests were designed with complex loading modes using the specially-designed testing machine introduced in Fig. 3(b). The tests were conducted under BWR coolant conditions with a DO concentration of 2 ppm using the loading modes shown in Fig. 42[49]. No acceleration of the crack growth rate was obtained for low alloy steel. Since the SCC phenomenon is time dependent, the da/dN data were replotted in the form of da/dt, as shown in Fig 43[49]. This figure clearly shows that the crack growth rate under mode 3 loading corresponds to that under mode 1 loading, which indicates little acceleration. This could be due to the small contribution of SCC propagation, considering that the mode 2 loading curve shows a crack growth rate two orders of magnitude lower than that of mode 1 loading. The quasi-brittle patterns observed on the frac-

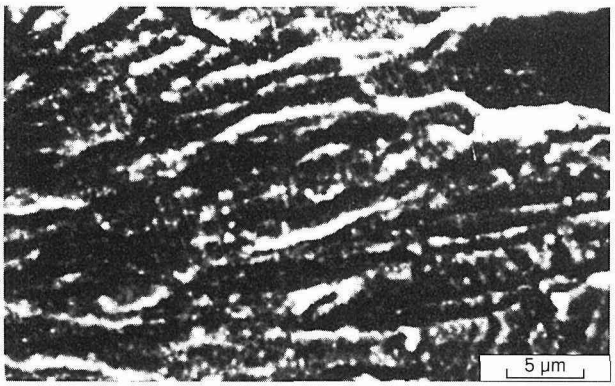

Fig. 44 Fracture surface of the specimen loaded under mode 3 in Fig. 42

ture surface, such as shown in Fig. 44[49], suggest the possibility of CF-SCC interaction of low alloy steels under complex loading modes and an even greater possibility for austenitic stainless steels, which have a higher susceptibility to SCC.

7. Mechanism of EAC in LWR Coolant Environments

Although a number of mechanisms have so far been proposed for explaining EAC phenomena in high temperature aqueous solutions, no unified mechanism of EAC in LWR coolant environments has been established because of the diversity of materials used for LWR components and of the EAC phenomena. As far as ferritic steels such as carbon steels and low alloy steels, SCC and CF phenomena are considered to be essentially governed by a single controlling mechanism, i. e., the crack initiates at a corrosion pit which is formed by the local fracture of oxide film. Impediment of repassivation, which is caused by the decrease of pH at the crack tip due to dissolution of manganese sulfide, may act as a dominant cause of corrosion pit formation. Hydrogen embrittlement also seems to cause crack growth acceleration. The film rupture and hydrogen cracking mechanisms are well accepted micromechanistic models for explaining EAC phenomena in high temperature water environments. However, it has been difficult to differentiate experimentally between these two mechanisms[50]. Since EAC results have so far been analyzed quantitatively by the film rupture mechanism, prediction of crack propagation in various environments has been successful using this model[51]. However, as already presented by Hanninen et al.[52] and also shown in Fig. 45[43], there is evidence of brittle failure that appears to be due to hydrogen induced cracking. Although the hydrogen cracking mechanism lacks quantitative validation, the formulation of an EAC phenomenological model might not be necessary for describing the controlling mechanism. The present results clearly show that crack growth acceleration does not occur without the dissolution of MnS inclusions, as shown in Fig. 39. In addition, the electrochemical potential at flow rate change tests decreases more rapidly for the medium sulfur steel than for the low sulfur steel, as mentioned before. There appears to be no doubt that dissolution of sulfide inclusions enhances the crack tip growth rate by hydrogen generation and permeation by a hydrogen embrittlement mechanism[52]. Much effort is needed to obtain data to quantify EAC phenomena and arrive at an elegant model.

8. Application of EAC Data

Along with progress in the acquisition of EAC data, the establishment of an EAC database has been demonstrated both domestically and internationally through the activities of groups such as ICCGR. Part of the corrosion fatigue data produced by NRIM was input into EDEAC (the EPRI Database for Environmentally Assisted Cracking), which was established by the Electric Power Research Institute of the USA, and into domestic databases such as FADAL (FAtigue DAta Library), which was established by the Japan High Pressure Technology Institute, and JMPD (JAERI Material Performance Database) for nuclear reactor materials, which was established by the Japan Atomic Energy Research Institute. EDEAC and FADAL will be used as supporting data for a future revision of the design fatigue curves in the ASME Code, Secs. III and XI. NRIM itself launched the development of materials life prediction technology in 1987. A consolidated database of material strength, including creep, fatigue and the effect of corrosive environments, is being developed along with an advanced, integrated database management system, named DIMS (Dialogical Integrated system for Material Strength database)[53]. Although the database is still in progress, EAC data from NRIM studies will be compiled in the next stage of program development.

These databases may serve as a strong basis for the revision of Secs. III and XI of the ASME Code. A major aim of the ICCGR activity focuses on improvement of the

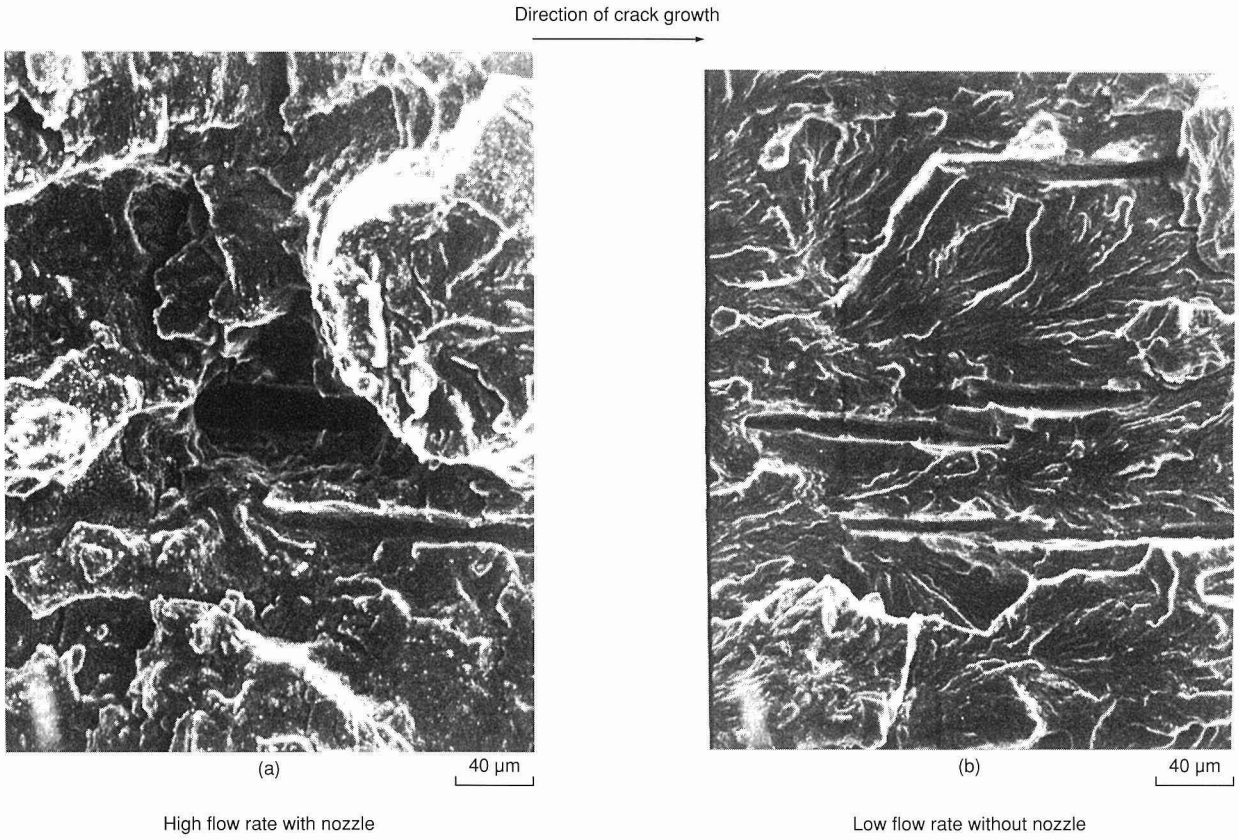

Fig. 45 Typical examples of microscopic fracture surfaces of medium sulfur low alloy steel fatigued in high temperature water at different flow rates

Code, especially the flaw evaluation curves of Sec. XI, Appendix A. The present results show that low alloy steels behave with a significant margin from the reference crack growth curves under BWR and PWR coolant conditions. However, some results indicate a poor margin by influential variables such as a high sulfur content of the steel, high DO concentrations, stagnant flow and temperature dependence. Damage acceleration due to CF-SCC interaction may also be expected. The present results also show a strain rate effect, which may be a problem for the design fatigue curves in ASME Sec. III. Some data are expected at points below the design fatigue curves when the components have cyclic loading at strain rates lower than that used in laboratory tests. Tedious, time-consuming tests have to be performed to prove the complete dependence. Basically, there is no factual correlation between the design fatigue curves and the fatigue lives of actual components. Thus, material data that falls below the design curves does not mean that damage to the component will occur. Since LWR components constructed to date possess a wide variety of material compositions and coolant conditions, the possibility of such influential conditions existing should not be ignored. Quantification of material behavior under these environments must be envisaged. Fruitful results from these efforts may bring about further development of the safety of nuclear energy.

9. Concluding Remarks

NRIM has so far contributed to the study of EAC problems of LWR structural materials especially in the field of engineering data acquisition for a decade. However, recent general trends of the materials research lead us to shift our interests to the fundamental research. This seems indeed to be one of the directions for the development of the EAC research. Technical issues which can work as a breakthrough for the relevant research are as follows: 1) Development of micro-electrodes available in high temperature water for the evaluation of water

chemistry in local environments at corrosion pit, crack tip and crevice. 2) Quantitative analysis of the amount of hydrogen and identification of the diffusion path of hydrogen, which arises from the cathodic reaction in high temperature water, to clarify the mechanism of hydrogen embrittlement. Furthermore, following future works are expected for further development of the analysis of EAC and data acquisition. One is the elucidation of the elemental process of local damage and the other computer simulation based on knowledge-databases. The former aims at clarifying the initiation process of local damage through the wide range analysis from macroscopic to atomic levels by using scanning probe microscopy such as scanning tunneling microscope and atom force microscope combined with electrochemical procedures. The latter may extend to the estimation of material strength in high temperature water by computer simulation based on the knowledge-databases especially in the case of time consuming experimental works. The author believes that these efforts would contribute to the further development of materials science and research in the field of EAC problems.

Acknowledgements

The author would like to express his hearty thanks to his colleagues, Drs. T. Ishihara and Y. Katada, Mrs. S. Matsushima and Messrs. S. Sato and S. Ohashi, who have engaged in the project for the national research programs of reactor safety established by the Science and Technology Agency.

References

1) K.E. Stahlkopf: *Structural Integrity of Light Water Reactor Components*, ed. by L.E. Steele, K.E. Stahlkopf and L.H. Larsson, Applied Science Publishers, London (1982), pp.29–54.
2) B. Byas et al.: Nucl. Tech., **55** (1981), 525.
3) T. Kondo et al.: *Corrosion Fatigue*, ed. by Staehle, NACE, (1972), 539.
4) T. Kondo et al.: 6th Ann. Int. conf. HSST, (1972), ORNL, USAEC.
5) B. Tomkins: Int. J. Pres. Ves. & Piping, **40** (1989), 331.
6) ASTM Standard E399.
7) ASTM Standard E647.
8) A. Saxena and S. J. Hudak, Jr.: Int. J. Fracture, **14** (1978), 453.
9) T. Ishihara: Unpublished.
10) T. Ishihara, S. Matsushima, S. Ohashi and Shimizu: J. Japan Inst. Metals, **41** (1977), 596 (in Japanese).
11) S. Matsushima, T. Ishihara, S. Ohashi and G. Ito: Trans. Nat. Res. Inst. Metals, **21** (1979), 13.
12) H.H. Klepfer et al.: GE Report, No. NEDO21000-1 (1975).
13) T. Ishihara and S. Ohashi: Trans. Nat. Res. Inst. Metals, **27** (1985), 130.
14) J.N. Kass, W.L. Walker and A.J. Giannuzzi: Corrosion, **36** (1980), 299.
15) S. Ohashi and T. Ishihara: J. Japan Inst. Metals, **54** (1990), 919 (in Japanese).
16) S. Matsushima and Y. Shimizu: Boshoku-Gijutsu, **32** (1983), 442 (in Japanese).
17) S. Matsushima and Y. Shimizu: Trans. Japan Inst. Metals, **24** (1983), 149.
18) Y.P. Ding, S. Matsushima, S. Sato and N. Nagata: Corr. Eng., **39** (1990), 137.
19) F.P. Ford: EPRI NP-2406 (1982).
20) F. Umemoto and T. Kawamoto: Boshoku-Gijutsu, **30** (1981), 276 (in Japanese).
21) T. Ishihara and S. Ohashi: Boshoku-Gijutsu, **37** (1988), 417 (in Japanese).
22) S. Ohashi and T. Ishihara: Corr. Eng., **41** (1992), 271–80.
23) ASME: Boiler and Pressure Vessel Code, Sec. III, ASME, New York, (1986).
24) W.H. Bamford: ASME J. Eng. Mater. & Tech., **101** (1979), 182.
25) B. Tomkins: Int. J. Pres. Ves. & Piping, **40** (1989), 331.
26) H. Kitagawa, H. Nakajima, N. Nagata, Y. Sakaguchi and T. Iwadate: Proc. 2nd IAEA Specialists' Meeting on Subcritical Crack Growth, Sendai, NUREG/CP-0067, **1** (1986), 135.
27) N. Nagata, S. Sato and Y. Katada: ISIJ Int., **31** (1991), 106.
28) N. Nagata, S. Sato and Y. Katada: Trans. 10th Int. Conf. on SMiRT, **F** (1989), 209.
29) G. Nakao, H. Yamasaki, S. Kimura, A. Nishioka, M. Yamaguchi and Y. Miura: Proc. Corr. Symp., Japan Soc. Corr. Eng., Tokyo, (1983), 20 (in Japanese).

30) M. Higuchi and H. Sakamoto: Tetsu-to-Hagane, **71** (1985), 1025 (in Japanese).
31) K. Iida, H. Kobayashi and M. Higuchi: Proc. 2nd IAEA Specialists' Meeting on Subcritical Crack Growth, Sendai, NUREG/CP-0067, **2**, (1986), 385.
32) W.A. Van Der Sluys and R.H. Emanuelson: ibid., **1**, 199.
33) J.D. Atkinson and J.E. Forrest: ibid., **2**, 153.
34) T. Kawakubo and M. Hishida: Corrosion-NACE, **40** (1984), 120.
35) Y. Katada, N. Nagata and S. Sato: Int. J. Pres. Ves. & Piping, **48** (1991), 37.
36) K. Katada and N. Nagata: Corr. Sci., **25** (1985), 693.
37) N. Nagata and Y. Katada: Trans. 9th Int. Conf. on SMiRT, **F** (1987), 167.
38) J.D. Atkinson, S.T. Cole and E. Forrest: Proc. IAEA Specialists' Meeting on Subcritical Crack Growth, Freiburg, NUREG/CP-0044, **2** (1983), 173.
39) T.A. Prater and L.E. Coffin: ibid., **2**, 355.
40) W.H. Cullen, K. Törrönen and M. Kempainen: NUREG/CR-3230 (1983).
41) Y. Katada, N. Nagata and S. Sato: ISIJ Int., **33** (1993), 877.
42) D.R. Tice, J.D. Atkinson and P.M. Scott: Proc. 2nd IAEA Specialists' Meeting on Subcritical Crack Growth, Sendai, NUREG/CP-0067, **1** (1986), 251.
43) Y. Katada, N. Nagata and S. Sato: J. Soc. Mater. Sci. Japan, **41** (1992), 1648 (in Japanese).
44) G. Gabetta and G. Buzzanca: Proc. 2nd IAEA Specialists' Meeting on Subcritical Crack Growth, Sendai, NUREG/CP0067, **2** (1986), 219.
45) P. Combrade, M. Foucault and G. Slama: ibid., **2**, 201.
46) H. Choi, F.H. Beck, Z. Szklarska-Smialowska and D.D. MacDonald: Corrosion, **38** (1982), 136.
47) S. Matsushima, Y. Katada, S. Sato and N. Nagata: Zairyou-to-Kankyou, **42** (1993), 636 (in Japanese).
48) S. Sato, N. Nagata and Y. Katada: Corr. Eng., **40** (1991), 391.
49) N. Nagata, T. Ishihara, S. Matsushima, Y. Katada, S. Sato and S. Ohashi: NRIM Kenkyu-Houkokusyu (Report of NRIM), **14** (1993), 29 (in Japanese).
50) W. Cullen, G. Gabetta and H. Hanninen: NUREG/CR-4422, (1985).
51) F.P. Ford: Int. J. Pres. Ves. & Piping, **40** (1989), 343.
52) H. Hanninen, K. Törrönen, M. Kempainen and S.Salonen: Corr. Sci., **23** (1983), 663.
53) M. Nihei and T. Konno: Trans. Jap. Soc. Mech. Eng., **58** (1992), 1287 (in Japanese).

Environmentally Assisted Cracking of Structural Materials for Light Water Reactors

by

Norio NAGATA

NRIM Special Report
(Research Report)
No. 94-01

Date of issue: 31 March, 1994

Publisher, Contact:
Toshikazu ISHII
Planning Section, Administration Division
National Research Institute for Metals
2–3–12, Nakameguro, Meguro-ku, Tokyo 153, Japan
Phone: +81-3-3719-2271 Fax: +81-3-3792-3337

Typeset using the SGML by Uniscope, Inc., Tokyo

Environmentally Assisted Cracking of Structural Materials for Light Water Reactors

by
Norio NAGATA

NRIM Special Report
(Research Report)
No. 94–01

Contents

Abstract 1
1. Introduction 2
2. Environmental Degradation of LWR Components 2
2.1 SCC of Austenitic Stainless Steel Piping 2
2.2 SCC and CF of SG Tubing 3
2.3 Fatigue Failure in Carbon Steel Piping 3
2.4 CF of Low Alloy Steel for RPV 3
3. Framework of EAC Research by NRIM 3
4. Experimental Techniques 3
5. SCC of Structural Materials for LWRs 8
5.1 SCC of Austenitic Stainless Steels 9
5.1.1 Temperature dependence 9
5.1.2 Effect of heating and cooling rates 10
5.1.3 Effect of environmental and loading transients 10
5.1.4 Role of oxide film on SCC 11
5.2 SCC of High Nickel Alloys 12
5.3 SCC of Carbon Steels 13
6. CF of Low Alloy Steels 16
6.1 Low Cycle Fatigue 16
6.1.1 Effect of high temperature water environment on S-N curves 17
6.1.2 Comparison with ASME Code, Sec. III 18
6.1.3 Origin of fatigue cracking in high temperature water 18
6.2 Fatigue Crack Growth 19
6.2.1 Direct observation of cracking in high temperature water 19
6.2.2 Effects of variables on fatigue crack growth rates 20
6.3 Interaction of CF and SCC in Low Alloy Steel 27
7. Mechanism of EAC in LWR Coolant Environments 28
8. Application of EAC Data 28
9. Concluding Remarks 29
Acknowledgements 30
References 30